AD-A165 149 DEVELOPMENT AND OPERATING CHARACTERISTICS OF THE PS132 1/1
THERMAL BATTERY(U) HARRY DIAMOND LABS ADELPHI MD
F C KRIEGER JAN 86 HDL-TR-2075

UNCLASSIFIED F/G 11/6 NL

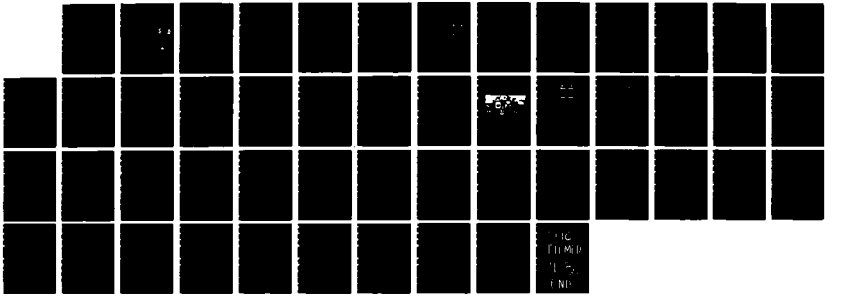

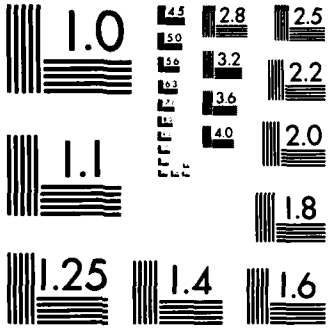

MICROCOPY RESOLUTION TEST CHART
NATIONAL BUREAU OF STANDARDS-1963-A

(12)

HDL-TR-2075
January 1986

AD-A165 149

Development and Operating Characteristics of the PS132 Thermal Battery

by Frank C. Krieger

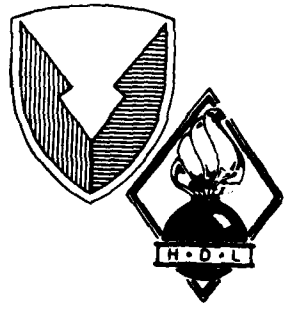

U.S. Army Laboratory Command
Harry Diamond Laboratories
Adelphi, MD 20783-1197

The findings in this report are not to be construed as an official Department of the Army position unless so designated by other authorized documents.

Citation of manufacturers' or trade names does not constitute an official indorsement or approval of the use thereof.

Destroy this report when it is no longer needed. Do not return it to the originator.

REPORT DOCUMENTATION PAGE

READ INSTRUCTIONS BEFORE COMPLETING FORM

1. REPORT NUMBER: HDL-TR-2075
2. GOVT ACCESSION NO.: ADA165149
3. RECIPIENT'S CATALOG NUMBER:

4. TITLE (and Subtitle): Development and Operating Characteristics of the PS132 Thermal Battery
5. TYPE OF REPORT & PERIOD COVERED: Technical Report
6. PERFORMING ORG. REPORT NUMBER:

7. AUTHOR(s): Frank C. Krieger
8. CONTRACT OR GRANT NUMBER(s):

9. PERFORMING ORGANIZATION NAME AND ADDRESS:
Harry Diamond Laboratories
2800 Powder Mill Road
Adelphi, MD 20783-1197
10. PROGRAM ELEMENT, PROJECT, TASK AREA & WORK UNIT NUMBERS: Program Ele: 65801A

11. CONTROLLING OFFICE NAME AND ADDRESS:
U.S. Army Materiel Command
5001 Eisenhower Avenue
Alexandria, VA 22333-0001
12. REPORT DATE: January 1986
13. NUMBER OF PAGES: 48

14. MONITORING AGENCY NAME & ADDRESS (if different from Controlling Office):
15. SECURITY CLASS. (of this report): UNCLASSIFIED
15a. DECLASSIFICATION/DOWNGRADING SCHEDULE:

16. DISTRIBUTION STATEMENT (of this Report):
Approved for public release; distribution unlimited.

17. DISTRIBUTION STATEMENT (of the abstract entered in Block 20, if different from Report):

18. SUPPLEMENTARY NOTES:
HDL Project: 49B540
AMS Code: 665801.M4500000
DA Project: 1P665801MM45

19. KEY WORDS (Continue on reverse side if necessary and identify by block number):
Thermal battery
DEB electrolyte-cathode calcium-lithium alloy

20. ABSTRACT (Continue on reverse side if necessary and identify by block number):

The development and operating characteristics of the PS132 thermal battery are described. The PS132 uses the electrochemical system Ca/LiCl-KCl eutectic-SiO_2/$CaCrO_4$, and it is one of the smallest batteries of its type ever built that can meet its electrical and environmental requirements. A development program that included construction of approximately 400 PS132-like batteries showed that obtaining acceptable DEB electrolyte-cathode powders was a major problem. Most commercial DEB powders caused excessive amounts of $CaLi_2$ molten metal to form in the operating thermal cells of the PS132. This molten metal then flowed from the cells and caused electrical short circuits.

CONTENTS

	Page
1. INTRODUCTION	5
2. DEVELOPMENT OF THE PS132 THERMAL BATTERY	6
3. PS132 FINAL-DESIGN BATTERY	17
4. SUMMARY AND CONCLUSIONS	26
LITERATURE CITED	28
APPENDIX A.--HEAT-TRANSFER ANALYSIS OF THE PS132 THERMAL BATTERY	29
DISTRIBUTION	45

FIGURES

1. PS132 thermal battery	5
2. Typical failure mode for PS132 thermal battery	8
3. End cell temperature and battery voltage for PS132 prototype forerunner (ambient temperature, 60 C)	9
4. Center cell and battery case temperature for PS132 prototype forerunner (ambient temperature, 60 C)	9
5. Pulse-box load programmer for PS132 thermal battery	14
6. Assembled PS132 thermal battery and component parts	20
7. PS132 thermal battery	21
8. Internal PS132 thermal battery resistance versus discharge time	24

TABLES

Page

1. Stack Construction of PS132 Prototype Forerunner Battery 10

2. Stack Construction of PS132 Prototype Battery 11

3. Electrical Performance of PS132 Final-Design Batteries Operating without the Anodic Acetate Dip 15

4. Electrical Performance of PS132 Prototype Batteries 17

5. Stack Construction of PS132 Final-Design Battery 19

6. Internal Resistance of PS132 Final-Design Batteries 23

7. Internal PS132 Final-Design Battery Resistance versus Discharge Time 24

8. Electrical Performance of PS132 Final-Design Batteries 25

1. INTRODUCTION

The PS132 thermal battery (fig. 1) was developed at Harry Diamond Laboratories (HDL) for a Navy program: the semi-active laser-guided projectile (SALGP) program for the 5-in. rifle. This task was assigned to HDL by the Naval Surface Weapons Center (NSWC), Dahlgren, VA. HDL began developing the battery in March 1976. Ten prototype PS132 batteries were to be supplied to NSWC Dahlgren by September 1976, and a total of 210 final-design batteries was to be built by December 1977. Of these 210 batteries, 110 would be supplied to NSWC Dahlgren. The remaining batteries would be tested or held in storage for future study at HDL.

A thermal battery was chosen for this application because the SALGP spin rate (20 rps) would not develop sufficient force to distribute the electrolyte into the cells of a liquid-electrolyte reserve battery. With a thermal battery, the electrolyte is placed directly into each cell during construction, and no spin forces are required for subsequent electrolyte distribution.

Figure 1. PS132 thermal battery.

No significant chemical degradation occurs in a thermal cell during extended storage (25 yr), even though the electrolyte is inside the cell. With the liquid-electrolyte reserve systems, extended storage times can only be obtained by holding the electrolyte in an ampule isolated from the cells. The thermal battery electrolyte, however (usually LiCl-KCl eutectic, melting point 352 C), is frozen solid at all anticipated storage temperatures (-54 to +74 C), so the cells remain chemically inert during storage. When a thermal battery is to be activated, a pyrotechnic heat source within each cell raises the cell temperature to 400 to 600 C, the frozen electrolyte melts, and the battery operates as any other voltaic battery system, until the cells cool below their minimum operating temperature.

Because of the high cell temperatures and the limited space available for thermal insulation, the cells in ordnance thermal batteries cool rapidly, and battery lifetimes are usually short (5 min or less). The lifetime required for the PS132 (160 s) was well within this limit. With special thermal insulation and an increased battery size, ordnance-type thermal batteries have been made that operate for an hour or more.[1]

[1] D. Bush, A Sixty-Minute Thermal Battery, Sandia Laboratories, Albuquerque, NM, SAND 75-0454 (March 1976).

The PS132 was required to activate in the absence of an electrical firing pulse. This was done with an inertial starter. The White (inertial) starter is a small mechanical device that was placed in the center hole of the PS132 cell stack. The White starter does not function under rapid shock conditions (drop of 40 ft onto steel), but does function under sustained shock (~575 g for ~2 ms), as in a gun launch. The White starter produces a spark that ignites the thermal battery pyrotechnic materials and activates the battery. An auxiliary starting mechanism was used for bench testing. This was a Nichrome wire buried in the pyrotechnic material. The wire was attached between terminals M and C (fig. 1) using nickel ribbon leads. The battery was activated by a capacitor discharged through the Nichrome wire.

The geometric, environmental, and electrical requirements for the PS132 were all designated by NSWC Dahlgren. Noting the high reliability of thermal batteries (usually greater than 99.9 percent at a 90-percent confidence level[2]), NSWC engineers allowed less space than would ordinarily be permitted for a battery with the PS132 requirements. Navy engineers believed that since the batteries operated so well it must be possible to make them smaller. The PS132 case bottom contained a threaded screw as an integral part. This screw mated with a forward bulkhead in the fuze. In actual operation, therefore, the PS132 was mounted upside down, and on gun launch the setback acceleration was against the case top. Ordinarily, a battery case would sit on top of a bulkhead in a fuze, and the bulkhead would supply much of the mechanical support required at gun launch. Because the PS132 did not have such mechanical support, both ends of the battery case were required to be significantly thicker than for most thermal batteries. This allowed still less space for a battery design that was already space-starved. As a result, the choice of design parameters for the PS132 was much more critical than for most batteries of its type.

2. DEVELOPMENT OF THE PS132 THERMAL BATTERY

The PS132 was required to deliver 18 to 26 V and to operate at a nominal current of 15 mA for a minimum required lifetime of 160 s. At some time during discharge, a pulse current of 1 to 2.5 A (6.0-ohm load) was applied for 64 ms. This pulse was followed by 250 ms of the nominal 15-mA drain, after which a second pulse current slightly greater than the first (4.6-ohm load) was drawn for 32 ms. Although the required steady-state current was only 15 mA, a 100-mA drain from the battery was maintained with a shunt resistor. This helped to prevent short-life battery failure, as will be explained below in this section.

The PS132 was to be activated nonelectrically, with setback on gun launch at 2000 to 8000 g and activation time to 18 V to be 150 to 250 ms. The required ambient temperature range was -40 to +140 F (-40 to +60 C), later reduced to -25 to +140 F (-32 to +60 C). The maximum required spin rate was 20 rps. The battery case was to be a right circular cylinder, 1.625 in. in

[2] M. Templeman, Thermal Battery Discharge Characteristics, United States Naval Ordnance Laboratory, White Oak, MD, NOLTR 64-14 (February 1966).

diameter and 1.500 in. tall, excluding mechanical and terminal protrusions from the case ends, specified by NSWC Dahlgren.

The PS132 was to use the conventional Ca/LiCl-KCl eutectic-SiO_2/$CaCrO_4$ electrochemical system. Nine thermal cells in series would deliver the proper voltage. The battery was to use pressed pellet technology,[1] with some slight modifications. Although many changes were made in battery design during the development, for purposes of discussion, this report condenses these changes into three basic battery types: (1) prototype forerunner, (2) prototype, and (3) final-design battery.

The development program soon showed that processing of the electrolyte-cathode powders for the PS132 was a major problem.[3,4,5] The PS132 electrolyte-cathode powder is a homogenous mixture of calcium chromate depolarizer (D), LiCl-KCl eutectic electrolyte (E), and SiO_2 binder (B). This powder is commonly called DEB powder and is used in many different mass-produced thermal batteries. With present DEB powder-processing techniques, approximately 60 percent of DEB powder batches made will produce thermal batteries that are highly reliable. The remaining 40 percent of the DEB powder batches will produce thermal batteries with high failure rates.

During development of the PS132 thermal battery, approximately 400 batteries were built and tested. Many of the initial batteries were built using a batch of DEB powder labeled A. This was a commercially obtained DEB powder that appeared to function well in the PS132 battery, but was not available in sufficient quantity for definitive testing. Sufficient quantities of this powder were not available to permit fabrication of the desired number (210) of PS132 thermal batteries. When other commercially obtained DEB powders were tried, frequent short-life battery failures of the type shown in figure 2 resulted. Eventually, a large batch (12.7 kg) of DEB powder was obtained from a commercial source. This batch, originally designated B, produced highly successful prototype forerunner batteries. Approximately 500 g of this powder, which was stored in a large glass jar, were removed from the top of the jar for testing. This powder was later found to be different from the rest of the B batch and was consequently redesignated B-1.

The commercial DEB powder source was requested to make a second batch of DEB powder identical to the B batch to test for reproducibility of manufacture. This powder was labeled C. When tested in the PS132 prototype forerunner design, DEB powder C produced frequent failures of the type shown in figure 2.

---

[1] D. Bush, A Sixty-Minute Thermal Battery, Sandia Laboratories, Albuquerque, NM, SAND 75-0454 (March 1976).

[3] C. Lofton et al, A Chemical and Physical Characterization of Calcium and Barium Chromates and Thermal Cell Performance of Calcium Chromates, Air Force Aeropropulsion Laboratory, Air Force Wright Aeronautical Laboratories, Wright Patterson Air Force Base, OH, AFAPL-TR-76-85 (April 1977).

[4] D. Bush, Electrolyte-Binder Powder Fusing Study, Sandia Laboratories, Albuquerque, NM, SC-TM-72-0651 (October 1972).

[5] R. Clark, Heat of Reaction Determinations in the System Ca-LiCl-KCl-$CaCrO_4$-SiO_2 Using Differential Scanning Calorimetry, Thermochim. Acta, 26 (1978), 49.

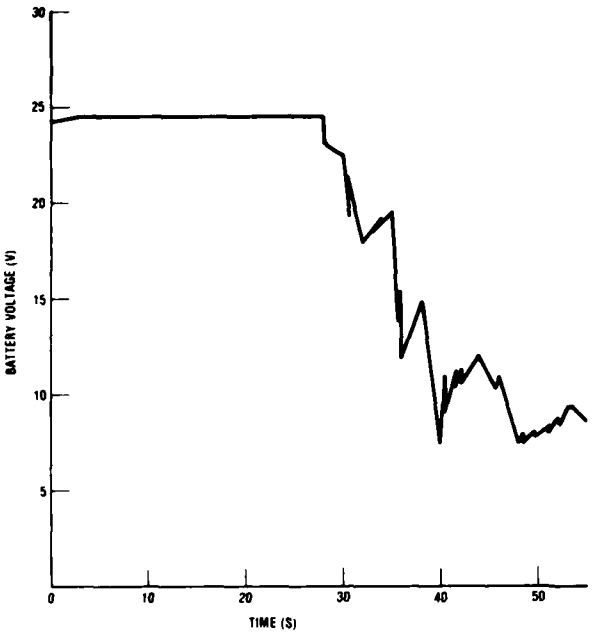

Figure 2. Typical failure mode for PS132 thermal battery.

Another DEB powder was obtained from the commercial source for testing in the PS132 prototype forerunner design. Batteries built using this powder (powder D) produced PS132 prototype forerunner batteries that failed almost invariably when fired at +60 C. Voltage-time traces for failed batteries were similar to the trace shown in figure 2.

The difficulty associated with obtaining acceptable DEB powder was partly caused by the fact that the PS132 is one of the smallest batteries of its kind ever built that can meet such stringent voltage, current, and lifetime requirements. The PS132 required lifetime, in particular, was unusually long for this size and type of thermal battery. This small size and long life were made possible by using thin electrochemical cells, low current density, and a high maximum cell operating temperature. Unfortunately, all these conditions contribute significantly to electrical short circuits caused by excessive amounts of $CaLi_2$ molten metal that form during thermal cell operation. These short circuits can be expected to produce battery failures such as shown in figure 2.

The high cell operating temperatures were confirmed experimentally by temperature-time and voltage-time curves for battery S-43, a forerunner of the PS132 prototypes (fig. 3, 4). Battery S-43 (table 1) used the B-1 DEB powder and was almost identical to the PS132 prototypes in construction (table 2). The S-43 temperature-time curves were obtained using iron-constantan thermocouples, previously calibrated to 0.5 percent of the value measured.

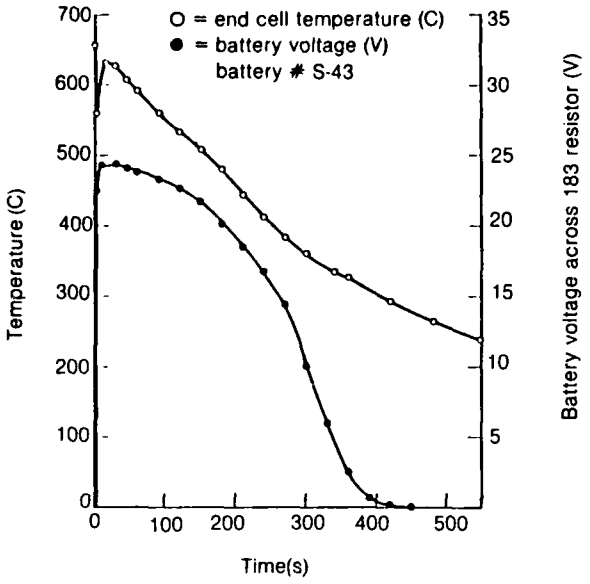

Figure 3. End cell temperature and battery voltage for PS132 prototype forerunner (ambient temperature, 60 C).

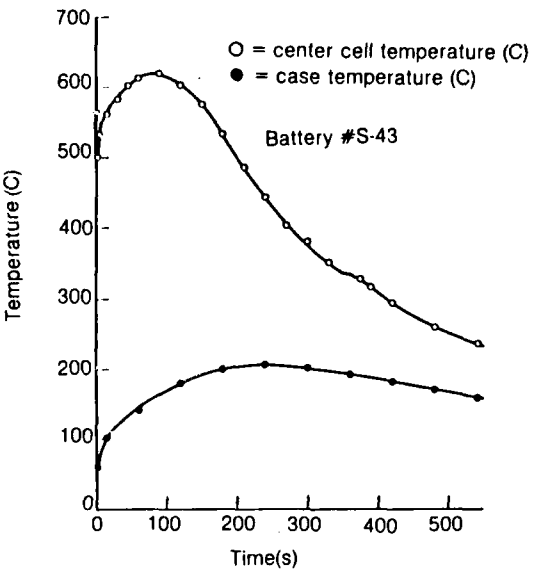

Figure 4. Center cell and battery case temperature for PS132 prototype forerunner (ambient temperature, 60 C).

The molten $CaLi_2$ which causes the electrical short circuits forms from a chemical side reaction during normal operation of the thermal cells. It is generally believed to be the effective anode of the Ca/LiCl-KCl eutectic-$SiO_2/CaCrO_4$ electrochemical system according to the following equations:

$$Ca \rightleftarrows Ca^{++} + 2e^{-} \qquad \text{Electrochemical anodic reaction} \qquad (1)$$

$$Ca + 2Li^{+} \rightleftarrows Ca^{++} + 2Li \qquad \text{Chemical side reaction} \qquad (2)$$

$$Ca + 2Li \rightleftarrows CaLi_2 \text{ (mp* 230 C)} \qquad \text{Chemical side reaction} \qquad (3)$$

$$CaLi_2 \rightleftarrows Ca^{++} + 2Li^{+} + 4e^{-} \qquad \text{Electrochemical anodic reaction} \qquad (4)$$

Many of the favorable discharge characteristics of the calcium anode in this system are believed to be a result of the constant renewal of the fluid $CaLi_2$ (mp* 230 C) at the calcium surface when the thermal cell is at its operating temperature of 400 to 600 C. As the operating temperature of the thermal cell increases, the rate of $CaLi_2$ formation increases according to the equilibria in equations (2) and (3). As the current drawn from the cell increases,

*mp = melting point

molten $CaLi_2$ is consumed electrochemically according to the equilibria in equation (4). Excess axial force on the cell causes molten $CaLi_2$ to be extruded at the cell edges. When conditions are such that molten $CaLi_2$ is formed and extruded faster than it can be consumed, the excess molten metal can bridge one or several cells, resulting in electrical short circuits.

TABLE 1. STACK CONSTRUCTION OF PS132 PROTOTYPE FORERUNNER BATTERY (BATTERY S-43) STACK FORCE, 200 lb

Component	Diameter (in.)		Thickness (in.)	Mass (g)
	Outer	Inner		
Bottom asbestos disk	1.50	--	0.033	0.723
Four asbestos rings	1.50	0.468	0.133	2.791
Half Fiberfrax ring	1.25	0.468	0.018	0.181
End heat pellet	1.25	0.442	0.065	4.558
Half Fiberfrax ring	1.25	0.468	0.018	0.177
Two asbestos rings	1.25	0.468	0.067	0.904
Half Fiberfrax ring	1.25	0.468	0.018	0.156
Electrochemical-heat source system				
Nickel positive collector	1.25	0.468	0.005	0.760
Ten heat pellets	1.25	0.442	0.166	11.643
Nine bimetal anodes	1.25	0.468	0.127	7.854
Nine DEB pellets	1.25	0.442	0.270	7.236
Nickel negative collector	1.25	0.468	0.005	0.760
Two nickel thermocouple rings (est)	1.25	0.468	0.010	1.51
Half Fiberfrax ring	1.25	0.468	0.018	0.167
Two asbestos rings	1.25	0.468	0.067	0.914
Half Fiberfrax ring	1.25	0.468	0.018	0.135
End heat pellet	1.25	0.442	0.065	4.588
Half Fiberfrax ring	1.25	0.468	0.018	0.141
One asbestos ring	1.25	0.468	0.034	0.452
Three asbestos rings	0.984	0.468	0.095	0.796
Top asbestos disk	0.984	--	0.033	0.311
Two Fiberfrax side wraps	--	--	--	2.615
Heat paper fuse train	--	--	--	0.854
Fiberfrax center wrap (est)	--	--	--	0.22
White starter	--	--	--	6.483

A number of methods can be used to reduce short circuits resulting from $CaLi_2$ molten metal formation. The most commonly used methods are to increase the current drain, decrease the cell operating temperature, and increase the electrolyte-cathode thickness.

TABLE 2. STACK CONSTRUCTION OF PS132 PROTOTYPE BATTERY (BATTERY W-17)
STACK FORCE, 350 lb

Component	Diameter (in.)		Thickness (in.)	Mass (g)
	Outer	Inner		
Two bottom asbestos disks	1.50	--	0.064	1.488
Four asbestos rings	1.25	0.468	0.133	1.749
Half Fiberfrax ring	1.25	0.468	0.018	0.127
Insulation heat pellet	1.25	0.442	0.065	4.677
Half Fiberfrax ring	1.25	0.468	0.018	0.164
Two asbestos rings	1.25	0.468	0.064	0.884
Half Fiberfrax ring	1.25	0.468	0.018	0.165
Electrochemical-heat source system				
Nickel positive collector	1.25	0.468	0.005	0.761
Ten heat pellets	1.25	0.442	0.170	12.302
Nine bimetal anodes	1.25	0.468	0.108	8.090
Nine DEB pellets	1.25	0.442	0.275	7.469
Nickel negative collector	1.25	0.468	0.005	0.760
Half Fiberfrax ring	1.25	0.468	0.018	0.157
Two asbestos rings	1.25	0.468	0.064	0.867
Half Fiberfrax ring	1.25	0.468	0.018	0.160
Insulation heat pellet	1.25	0.442	0.064	4.635
Half Fiberfrax ring	1.25	0.468	0.018	0.160
Four asbestos rings	1.25	0.468	0.136	1.751
Three asbestos rings	1.25	0.468	0.102	1.250
(Four 0.125-in.-diam. notches at 90° for lid tabs)				
Two top asbestos disks	1.25	--	0.065	0.980
(Four 0.125-in.-diam. notches at 90° for lid tabs)				
Two Fiberfrax side wraps	--	--	--	2.802
Heat paper fuse train	--	--	--	0.844
Asbestos center wrap	--	--	--	0.442
White starter	--	--	--	6.468

Typical values of these parameters for production Ca/LiCl-KCl eutectic-$SiO_2/CaCrO_4$ electrochemical cells are 300-mA/in.^{2} cell current density, 550-C maximum cell operating temperature, and 0.050-in. electrolyte-cathode thickness. The values of these parameters in the PS132 design are 100-mA/in.^{2} minimum cell current density, 630-C maximum cell temperature (fig. 3, 4), and 0.030-in. electrolyte-cathode thickness. From the discussion of equations (1) through (4) in this section, it is obvious that the PS132 will be more subject to $CaLi_2$ electrical short circuits than most batteries of its kind. The PS132 operating parameters cannot be changed, however, because of geometry and performance requirements.

Methods of processing the DEB powder are known to affect production of $CaLi_2$ electrical short circuits. Use of less binder, for example, increased the number of $CaLi_2$ electrical short circuits in this study. Baking times and temperatures contribute to $CaLi_2$ formation rates. The size distribution[6] of the DEB particle constituents or of the DEB powder itself would be expected to contribute to chemical uniformity of the DEB mixture and therefore to $CaLi_2$ formation rates. Additional calcium ions, usually $Ca(OH)_2$ or $CaCl_2$, may be placed in the DEB powder to drive the equilibria in equations (2) and (3) to the left, using LeChatelier's principle, thereby reducing $CaLi_2$ formation.[7,8]

The formation rate of $CaLi_2$ molten metal was reduced in the PS132 battery by dipping the pure calcium anodes into an 82/18-volume-percent solution of acetone/glacial acetic acid before battery construction. This coated the pure calcium surface with a calcium acetate layer. Calcium ions from the acetate layer will then be dissolved into the electrolyte when the cell is activated, driving the equilibria in equations (2) and (3) to the left.[9] In addition, less pure calcium will contact the electrolyte-cathode because much of the calcium surface is covered by acetates and oxycompounds of calcium. Both acetate and hydroxide coatings of the pure calcium surface have been used in this manner to reduce $CaLi_2$ formation rates.[9,10]

Tests were run in which PS132 battery stacks were activated outside the case so that the formation of $CaLi_2$ molten metal droplets could be seen. In these tests, droplets could be observed forming on the outer diameter of the stacks. The droplets grew steadily as the battery stacks continued to operate and in most cases eventually bridged the anode and cathode of a single cell. An intense spark was observed as that cell discharged electrically through the molten metallic $CaLi_2$. The resultant electrical heating increased the temperature of the molten metal, which then proceeded to flow down the cell stack, short-circuited several additional cells, and produced a voltage-time curve similar to that shown in figure 2. This was the major failure mode that had to be overcome in developing the PS132 thermal battery.

The rate of $CaLi_2$ molten metal formation in the open-stack tests was measured by allowing the units to cool, removing the $CaLi_2$ beads with forceps, and weighing them. This method of measuring $CaLi_2$ formation rates is often used in industry and is known to be reproducible within a factor of two. In these tests, $CaLi_2$ beads weighing 0.1 mg were easily observed and many proved to be large enough to cause electrical short circuits. Both the apparently successful DEB powder A and the highly unsuccessful DEB powder D were tested,

---

[6] R. Walton, A Chemical and Physical Characterization of Calcium and Barium Chromates and Thermal Cell Performance of Calcium Chromates, Air Force Aeropropulsion Laboratory, Air Force Wright Aeronautical Laboratories, Wright Patterson Air Force Base, OH, AFAPL-TR-79-2089 (November 1979).

[7] D. Bush, Thermal Battery, U.S. Patent 3,885,989 (27 May 1975).

[8] A. Baldwin, A Long-Life, Low Voltage, Power Thermal Battery, 26th Power Sources Symposium, PSC Publications Committee, Red Bank, NJ (1974), 137.

[9] R. Clark and K. Grothaus, Thermal Battery Having Protectively Coated Calcium Anode to Prevent Alloy Shorting, U.S. Patent 3,527,615 (8 September 1975).

[10] D. Bush, Thermal Battery, U.S. Patent 3,898,101 (5 August 1975).

and both of these powders produced 60 to 100 mg of $CaLi_2$ molten metal beads. This result suggests that the gas atmosphere inside an operating sealed battery may be important in reducing $CaLi_2$ formation rates. The mass of $CaLi_2$ formed from units constructed from the apparently successful DEB powder A when the units were fired in the open was 600 times that required to short-circuit a battery. When similar units constructed from DEB powder A were fired in the sealed battery case, no $CaLi_2$ formation was observed.

$Fe/KClO_4$ pyrotechnic powder is known to expel H_2O and other gases on ignition.[11] Most of the water will be in the form of vapor when the units are fired at high ambient temperature, because both the case and battery cells are at high temperature (fig. 4). For units fired at high ambient temperature, calculated gas pressures from the pyrotechnic gas evolution and heating were ~200 psi. If water is evolved from the heated DEB powder and thermal insulation also, the gas pressure will be higher. Gas pressure was not measured in operating units, but was known to be high. One PS132 development battery had a welding imperfection in the case, and when the unit was fired at high ambient temperature, the battery case ruptured so violently 310 ms after ignition that flying battery components destroyed an overhead light fixture.

The pressurized steam in the operating battery case would be expected to (1) react with $CaLi_2$ as it is formed and (2) react with the pure Ca anodes to inhibit $CaLi_2$ formation in the first place. The superior performance of the B-1 powder taken from the top of the large glass jar might be explained by assuming that the top portion of the B powder was slightly contaminated with water when the lid to the jar was opened or because the lid was not properly sealed. Powder A was the only other commercial powder that showed apparently good behavior in the PS132. This powder had been used intermittently in the laboratory for several years and could easily have become water contaminated.

Another indication of the importance of the gas atmosphere in the operating battery came from measurements of internal battery resistance. Use of the pulse-box load programmer (fig. 5) permits measurement of the battery internal resistance, R_i:

$$R_i = (E_2 - E_1)/(i_1 - i_2) \quad ,$$

where

R_i = internal battery resistance (ohms),

E_2 = battery voltage at top of pulse (volts),

i_2 = battery current at top of pulse (amperes),

E_1 = battery voltage at bottom of pulse (volts), and

i_1 = battery current at bottom of pulse (amperes).

[11] F. Bachner and C. Alexander, Techniques for Measuring Gas Evolved During Combustion of Pyrotechnic Heat Powders, Harry Diamond Laboratories, HDL-TM-68-4 (February 1968).

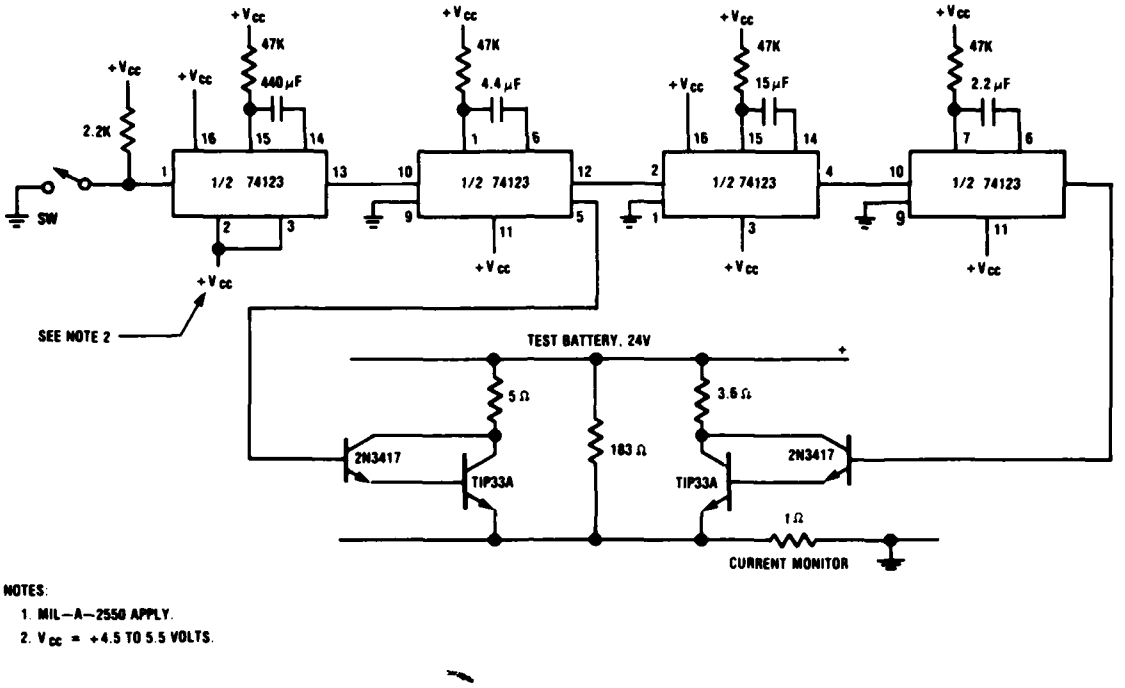

Figure 5. Pulse-box load programmer for PS132 thermal battery.

This equation is evaluated only during the instantaneous straight-line voltage drop when the pulse is applied and is a direct measure of internal battery resistance. Unfortunately, the equipment available had a response time of 1 to 2 ms compared with the response time of 1 to 2 μs that is often recommended for this measurement in this electrochemical system. Nevertheless, the 1- to 2-ms response measurement permitted a calculation of a maximum value for battery internal resistance, which may possibly be correlated with battery performance.

The effect of the gas atmosphere on the PS132 internal resistance was shown by constructing PS132 batteries in which the anodic acetate dip was omitted. In these units, the atmosphere in the sealed battery could react much more readily with the unprotected calcium anodic surface and any extruded $CaLi_2$ molten metal. The internal resistance of these batteries was measured with the pulse-box load programmer, and the results of these measurements are shown in table 3, along with battery performance.

For batteries fired at +60 C without the anodic acetate dip, life to 18 V was 70 to 75 s compared with ~280 s when the acetate dip was used. Battery internal resistance at 165 s for batteries fired at +60 C without the acetate dip was approximately three times that for identical units fired under identical conditions with the acetate dip.

TABLE 3. ELECTRICAL PERFORMANCE OF PS132 FINAL-DESIGN BATTERIES OPERATING WITHOUT THE ANODIC ACETATE DIP (PULSE-BOX LOAD, fig. 5, NOMINAL 100 mA/in.^{2} CELL CURRENT DENSITY)

Battery designation	Ambient temperature (C)	Stack force (lb)	Rise time to 18 V (ms)	Life to 18 V (s)	Battery internal resistance (ohms)		
					15 s	30 s	165 s
WE-211	+60	150	135	70	0.761	1.05	11.7
WE-212	+60	260	130	75	0.722	0.882	11.8
WE-237	-40	215	155	270	0.608	0.616	1.29

For the battery fired at -40 C without the acetate dip, life to 18 V was 270 s compared with ~180 s when the acetate dip was used. Battery internal resistance at 165 s for the battery fired at -40 C without the acetate dip was one-seventh that for an identical unit fired at -32 C with the acetate dip.

These results can be explained if we assume that water is expelled from the heated components when the batteries are activated. For units fired at +60 C, the water is in the vapor phase and reacts readily with the unprotected pure calcium, causing short battery lifetimes. The acetate coating on the units with the anodic dip protects the calcium from the water, resulting in longer battery lifetimes.

For units fired at -40 C, the water expelled from the heated battery components freezes on the battery case and is removed from the system. The calcium remains pure and reactive for units without the acetate dip fired at -40 C, and the electrochemical reaction is not slowed by dissolution of calcium ions into the electrolyte from the acetate dip, according to the equilibria in equations (2) and (3) above. For these units, battery internal resistance is lowered, and lifetime is increased.

Comparison of internal battery resistance and battery voltage at 165 s for units fired at +60 C shows that although resistance increased by a factor of 3 when no anodic dip was used, this increase in resistance was not sufficient to cause the dramatic decrease in voltage observed. Battery voltage at 165 s for units fired at +60 C with the acetate dip was typically 22 V compared with 16 V without the acetate dip. A decrease from 22 V to 16 V using the 184-ohm load in the load programmer would require a battery internal resistance of about 74.5 ohms, assuming a 4-ohm internal resistance often measured when the voltage was at 22 V with the acetate dip. This resistance is far greater than the 11.7- to 11.8-ohm values observed for the undipped units. This result shows that other types of polarization rather than simple resistive polarization are present, which is consistent with the loss of reaction sites on the calcium surface as pure calcium reacts with gases in the sealed battery case.

The gas atmosphere in the sealed battery also appears to react with the $CaCrO_4$ in the DEB pellet. This reaction was observed in another program, where DEB pellets from batteries fired at +60 C in sealed batteries were green, whereas DEB pellets for batteries fired at +60 C in unsealed containers retained their original yellow color.

In PS132 batteries fired at +60 C, the DEB pellet was mostly green (Cr_2O_3), compared with batteries fired at -40 C, where the DEB was mostly yellow ($CaCrO_4$). For the PS132 batteries fired at either +60 C or -40 C, less than 10 percent of the yellow $CaCrO_4$ is reduced electrochemically to the green, Cr_2O_3. These facts suggest that a chemical side reaction to produce green Cr_2O_3 may be taking place in the DEB pellet. Such a reaction would be expected to accelerate as the temperature of the operating cells increased because of the increase in the ambient temperature.

Both hydrogen gas and water vapor are known to exist in the sealed battery.[11] Although gas pressures are high, the molar amount of gases available to react with cell components is quite small. It is possible that a cyclic reaction sequence occurs in which reactions similar to

$$Ca + H_2O \rightarrow CaO + H_2 \quad (5)$$

$$3H_2 + 2CaCrO_4 \rightarrow 2CaO + Cr_2O_3 + 3H_2O \quad (6)$$

are repeated indefinitely until the cell's active components are exhausted. The exact contributions of anodic and cathodic polarization to total cell polarization in the sealed PS132 battery were not determined.

Heat transfer calculations on battery S-43, a PS132 prototype forerunner (see app A), confirmed that a significant amount of high-thermal-conductivity hydrogen gas was present in the operating sealed units.[12] These calculations also showed that significant amounts of heat were evolved from chemical side reactions in the operating thermal cells.

Although the measured temperature-time curves for battery S-43 showed that the thermal cells in the PS132 prototype forerunner and prototype designs of tables 1 and 2 are operating at much higher temperatures than are normally acceptable, these batteries performed acceptably so long as DEB powder B-1 was used. It was not possible to reduce the cell operating temperature significantly without unacceptably shortening the battery life when the units were fired at low ambient temperature. Accordingly, the construction of 24 PS132 prototype batteries using the B-1 DEB powder with the design shown in table 2 was started on 11 November 1976 and completed on 5 January 1977.

Of the 24 prototype batteries, 9 were randomly selected and tested at HDL using a resistive load of 183 ohms. No difficulty was noted in any test, and all batteries met the required performance; results are shown in table 4. The standard deviations in table 4 were calculated for a small number of sample sizes, as was done throughout this report to facilitate comparison of the results. When making statistical comparisons based on such calculations, it should be remembered that confidence levels will be low.

---

[11] F. Bachner and C. Alexander, Techniques for Measuring Gas Evolved During Combustion of Pyrotechnic Heat Powders, Harry Diamond Laboratories, HDL-TM-68-4 (February 1968).

[12] F. Krieger, Fusible Heat Reservoirs for Thermal Batteries, 26th Power Sources Symposium, PSC Publications Committee, Red Bank, NJ (May 1974), 129.

TABLE 4. ELECTRICAL PERFORMANCE OF PS132 PROTOTYPE BATTERIES (183-OHM RESISTIVE LOAD--NOMINAL 100 mA/in.^{2} CELL CURRENT DENSITY)

Battery designation	Ambient temperature (C)	Ignition method	Rise time to 18 V (ms)	Life to 18 V (s)
W3	+60	White starter	175	240
W17	+60	Electrical	173	241
W18	+60	Electrical	165	235
W19	+60	White starter	196	235
W2	+25	White starter	198	230
W1	-32	White starter	210	180
W4	-32	White starter	218	188
W7	-32	White starter	204	183
W11	-32	White starter	210	196
		Average battery lifetimes		
	+60 C	238 ± 3.2 s	($3.2 = \sigma_{n-1}$)	
	-32 C	187 ± 7.0 s	($7.0 = \sigma_{n-1}$)	
No electrical noise or battery difficulty in any test.				

Ten prototype batteries were supplied to the Navy for testing in January 1977, and the remaining five were stored at HDL. Prototype batteries tested by the Navy met all performance requirements without difficulty.

3. PS132 FINAL-DESIGN BATTERY

After the PS132 prototypes were delivered, attempts were made to improve the PS132 design. These consisted of altering (1) the battery current drain, (2) the amount of pyrotechnic material in the cells (and hence the cell operating temperature), (3) the dimensions, preparation, and placement of the thermal insulation and pyrotechnic materials, (4) the DEB electrolyte-cathode powders and their pressed pelletized densities, (5) the axial force on the cell stack, and (6) the inner and outer diameters of the bimetal anodes. These parameters were all varied such that molten $CaLi_2$ formation and flow would be minimized while still meeting PS132 requirements. The major objective was to develop a PS132 design that could use DEB powder C, which had supposedly been processed identically to DEB powder B. Although this study developed useful information, no design change could be found that made the use of DEB powder C possible.

In September 1977, construction began on the 210 final-design PS132 batteries. These first "final-design" batteries used the only design that had been proven successful at this point--the prototype design (table 2) using the B-1 DEB powder. When construction of the 210 final-design batteries began,

the B-1 DEB powder, taken from the top of the large glass B-DEB powder jar, was believed to be identical to the rest of the B-DEB powder. However, it was soon found that all the B-1 DEB powder had been used. When PS132 batteries were made from powder farther down in the jar, frequent battery failures of the type shown in figure 2 began to appear.

Samples of a fifth commercial DEB powder (powder E), which was then being used in a successful production thermal battery (PS413), were obtained from the DEB powder source. When tested in the PS132 prototype design, powder E, like powder D, produced batteries that failed almost invariably when fired at +60 C.

Battery tests showed that although the B-DEB powder was not able to produce successful PS132 batteries, it was superior to any of the other available DEB powders for PS132 use. Efforts were therefore concentrated on making the B DEB powder batch suitable for use.

Because the B-1 and B-DEB powders were nonuniform in battery performance, some physical or chemical difference obviously existed between the powders. Improved mixing of the B-DEB powder would produce more physical and chemical uniformity and insure more reproducible battery behavior. Accordingly, a 3153-g sample of the powder was removed from the center portion of the large jar containing the original batch. This sample was rolled for 36 hr in an 8-liter ceramic mill using only a simple rolling action of 44 revolutions per minute to mix the powder (no balls present in the mill). This 3153-g sample was sufficiently large to make all the final design PS132 batteries.

The PS132 design was further improved using test results from the program completed after delivery of the prototype units. After 69 preliminary "final-design" batteries from the lot of 210 to be supplied to NSWC Dahlgren had been tested, a true final design was found (table 5). PS132 batteries made according to this design produced electrical performance quite similar to that of the PS132 prototype design when using DEB powder taken from the 3153-g sample of the B DEB powder batch.

Although the electrical performance of the PS132 prototype and final-design batteries was quite similar, the B-1 DEB powder from which the prototypes were made was superior to the 3153-g B DEB powder sample from which the PS132 final-design batteries were made. Four major changes from the prototype design were necessary in order to use the 3153-g B DEB powder sample successfully in the PS132 final-design batteries (tables 2 and 5). It was necessary to (1) add an extra asbestos ring between the large insulation heat pellet and the cell stack, (2) carefully center the bimetal center hole by using a metal template during punching, (3) with a metal sleeve, carefully align the DEB pellet, heat pellet, and bimetal rings during battery construction, and (4) reduce stack force from 350 lb maximum in the prototype units to 250 lb maximum in the final-design units.

The stack force exerted on the cells by the spring action of the asbestos and Fiberfrax against the battery lid was found to be very important. Excessive stack force caused electrolyte and molten $CaLi_2$ flow, with resultant

electrical short circuits. Insufficient stack force resulted in poor mechanical integrity and inadequate bimetal-DEB contact, with adverse effects on proper current flow. Stack force for the PS132 final-design batteries was defined as 100 to 250 lb.

TABLE 5. STACK CONSTRUCTION OF PS132 FINAL-DESIGN BATTERY (BATTERY WE-139) STACK FORCE, 200 lb

Component	Diameter (in.)		Thickness (in.)	Mass (g)
	Outer	Inner		
Two bottom asbestos disks	1.50	--	0.064	1.622
Three asbestos rings	1.25	0.468	0.096	1.380
Half Fiberfrax ring	1.25	0.468	0.018	0.159
Insulation heat pellet	1.25	0.442	0.065	4.756
Half Fiberfrax ring	1.25	0.468	0.018	0.145
Three asbestos rings	1.25	0.468	0.096	1.384
Half Fiberfrax ring	1.25	0.468	0.018	0.182
Electrochemical-heat source system (fig. 7(c))				
Nickel positive collector	1.25	0.468	0.005	0.756
Ten heat pellets	1.25	0.442	0.170	11.960
Nine bimetal anodes	1.25	0.468	0.108	7.793
Nine DEB pellets	1.25	0.442	0.270	7.503
Nickel negative collector	1.25	0.468	0.005	0.755
Half Fiberfrax ring	1.25	0.468	0.018	0.123
Three asbestos rings	1.25	0.468	0.096	1.364
Half Fiberfrax ring	1.25	0.468	0.018	0.184
Insulation heat pellet	1.25	0.442	0.065	4.533
Half Fiberfrax ring	1.25	0.468	0.018	0.137
One asbestos ring	1.25	0.468	0.032	0.434
Two thin asbestos rings	1.25	0.468	0.016	0.180
Two asbestos rings	1.25	0.468	0.064	0.728
(Four 0.375-in.-diam. notches at 90° for lid tabs)				
Two top asbestos disks	1.25	--	0.064	0.841
(Four 0.375-in.-diam. notches at 90° for lid tabs)				
Two Fiberfrax side wraps (fig. 7(a))	--	--	--	2.894
Heat paper fuse train	--	--	--	0.887
Asbestos center wrap	--	--	--	0.358
White starter	--	--	--	6.491

The operating temperatures of the final-design PS132 thermal cells at the stack ends are similar to, but slightly lower than, those of the S-43 end thermal cells (fig. 3) because of the extra asbestos ring between the insulation heat pellet and the cell stack ends. These lower end-cell operating temperatures help to reduce $CaLi_2$ electrical short circuits according to information obtained from the development program.

Figure 6 shows an assembled final-design PS132 battery and some PS132 components. The brass White starter in the center of the picture is 1.07 in. long and serves as an effective scale for the picture. An assembled PS132 is to the left of the White starter, and a finished PS132 final-design stack (table 5) is assembled onto an aluminum mandrel to the right of the White starter. Thermal cell components including (1) $Fe/KClO_4$ pyrotechnic heat pellet, (2) DEB electrolyte-cathode, and (3) bimetal anode previously dipped in glacial acetic acid/acetone are arranged in front of the White starter. The thicker $Fe/KClO_4$ pyrotechnic heat pellet used to heat the thermal insulation is in the front row between two asbestos thermal insulators. Drawings of the assembled PS132 final-design battery and its components are shown in figures 7(a), (b), and (c).

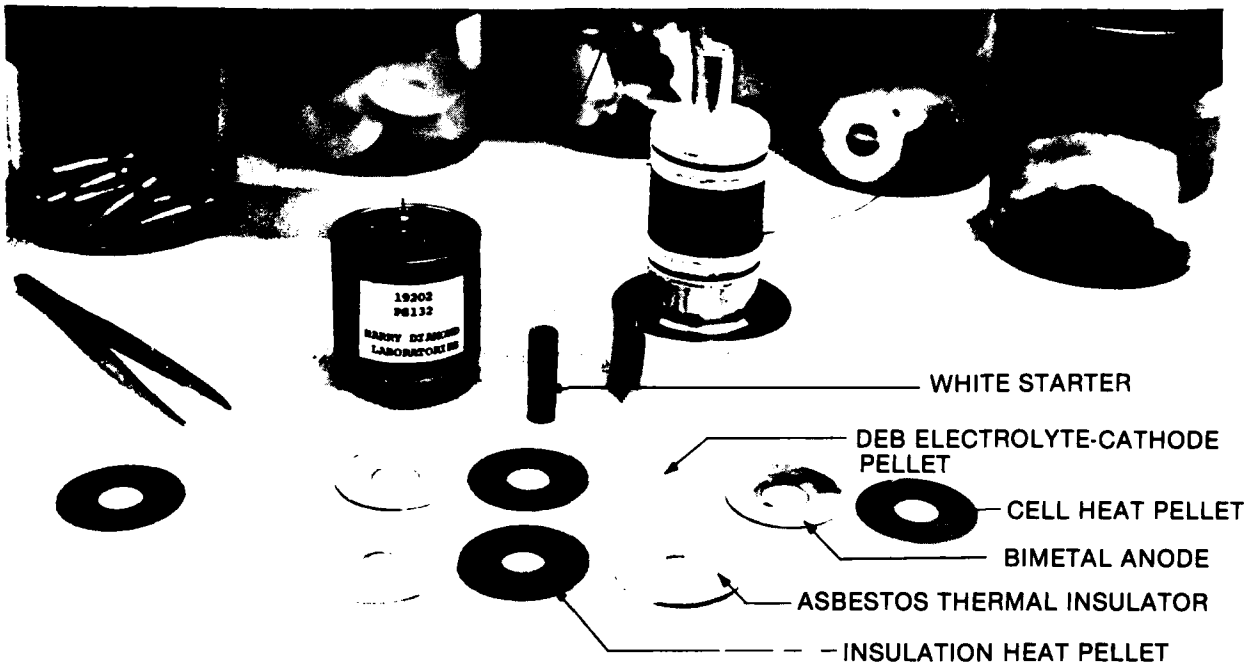

Figure 6. Assembled PS132 thermal battery and component parts.

The PS132 final-design thermal cells are in the form of annular disks (fig. 7(a) and (c) and table 5) and are activated on setback by a spark from a White starter located in the center hole. The spark ignites the heat paper fuse train, also located in the center hole, which, in turn, ignites the heat pellets (fig. 7(c)). The heat pellets in the cells are made by pelletizing 88/12 mass percent $Fe/KClO_4$ powder at a nominal force of 20 tons/in.^{2} to an apparent density of 4.0 g/cm^3. The mass of each cell heat pellet ranges from 1.16 to 1.24 g. Sufficient unreacted iron remains in the cell heat pellets after ignition to form intercell electrical connections. Ten heat pellets are required with the nine cells to achieve proper activation (fig. 7(c)). Current is drawn from the battery at the positive and negative nickel current collectors, which were previously baked 1 hr at 1100 F to remove traces of oil.

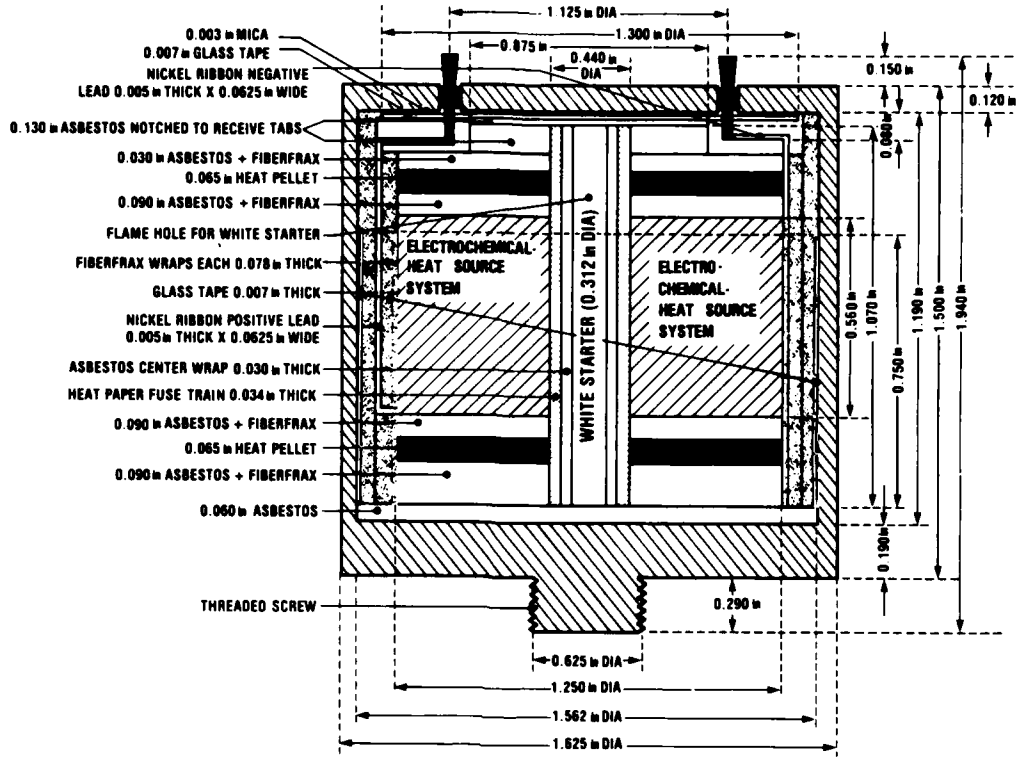

Figure 7(a). PS132 thermal battery: cross section.

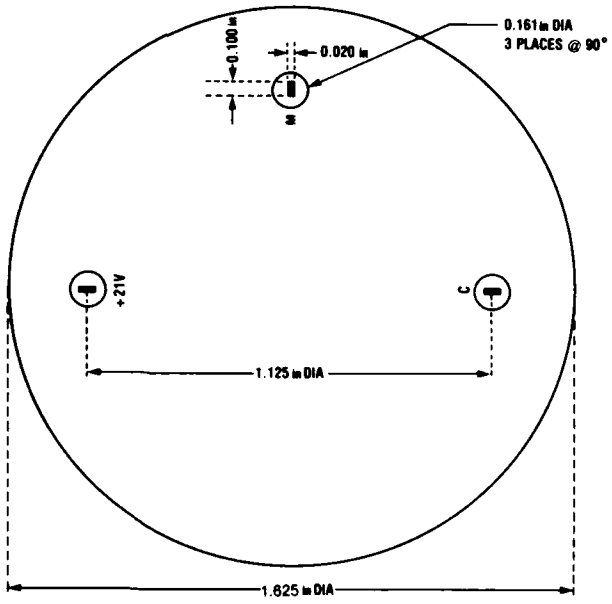

Figure 7(b). PS132 thermal battery: top view.

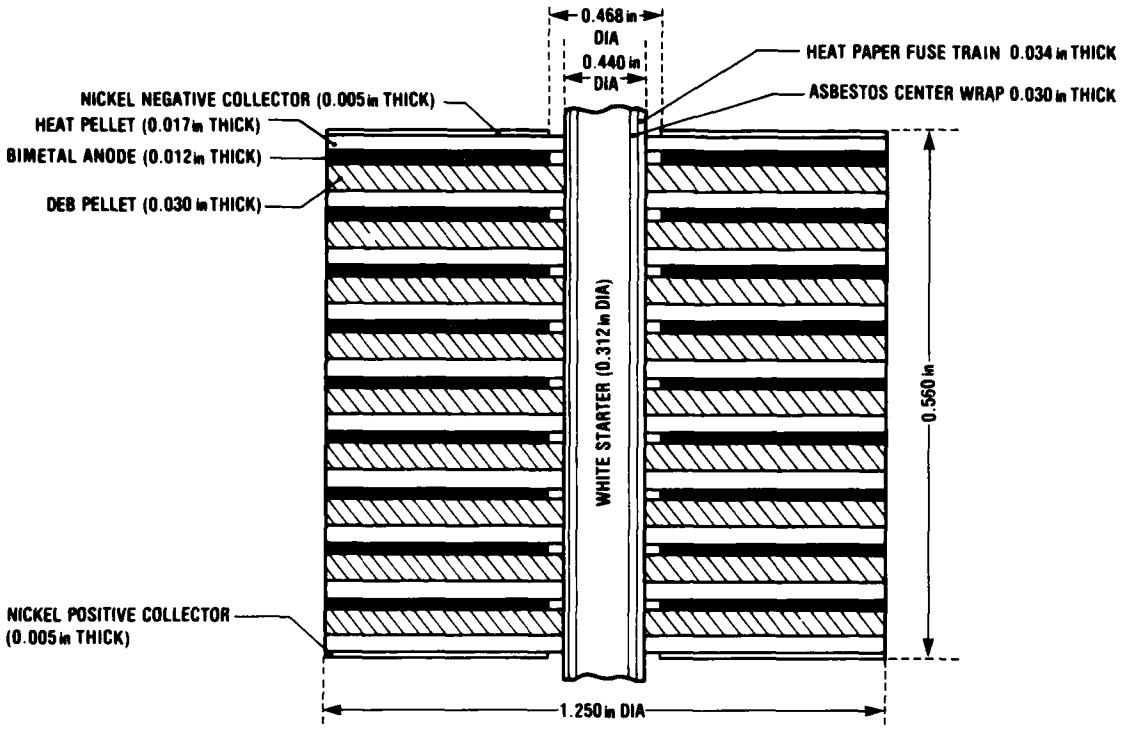

Figure 7(c). PS132 thermal battery: electrochemical-heat source system cross section (thickness of individual units varies by ±0.002 in.)

The PS132 final-design bimetal anodes consist of a base sheet of mild steel 0.005-in. thick on which calcium has been vapor deposited to a thickness of 0.007 in. The anodes were cut to size and then dipped into an 82/18 volume percent solution of acetone/glacial acetic acid and dried in vacuo before assembly. This combination formed a calcium acetate layer on the calcium surface which helped to reduce $CaLi_2$ electrical short circuits, as discussed in section 2. The i.d. of the bimetal (0.468 in.) was cut larger than the i.d. of the DEB pellet (0.442 in.). This procedure allowed any molten metallic $CaLi_2$ formed from the high initial temperature of the heat paper fuse train to flow into the resultant empty space, rather than into the battery center hole where it could cause electrical short circuits. The bimetal was not undercut at the stack o.d., where the outer Fiberfrax wrap helped to prevent $CaLi_2$ flow.

The PS132 final-design DEB pellet electrolyte-cathode was made from the 3153-g DEB powder sample taken from batch B. The DEB powder was pressed into the desired shape at a nominal force of 20 tons/in.^{2} to an apparent density of 1.6 g/cm^3. Each DEB pellet ranged from 0.8 to 0.9 g in mass. Chemical analysis of the DEB powder showed that it was 36.0/54.9/8.4 mass percent $CaCrO_4$/LiCl-KCl eutectic/SiO_2 (99.3 total mass percent).

The large heat pellets buried in the thermal insulation at each end of the battery stack (fig. 7(a)) were pelletized by pressing 86/14 mass percent

$Fe/KClO_4$ powder at a nominal force of 20 tons/in.^{2} to an apparent density of 4.0 g/cm^3. The mass of each of the insulation heat pellets ranged from 4.4 to 4.8 g. These heat pellets heat the thermal insulation and prevent excessive heat loss from the thermal cells to the insulation immediately following ignition. The asbestos and Fiberfrax insulations in the stack (table 5) were heated to 1100 F for 1 hr in an air atmosphere before assembly to remove organic binder and any water of hydration held in the asbestos. The outer Fiberfrax wraps (fig. 7(a)) were not baked before the batteries were assembled. Baking these wraps caused them to absorb electrolyte too readily and proved responsible for some battery failures.

Internal resistances of PS132 final-design batteries were measured by the pulse-box load method described in section 2. The results are shown in table 6. The battery voltage dropped to approximately 10 V when the pulses were

TABLE 6. INTERNAL RESISTANCE OF PS132 FINAL-DESIGN BATTERIES (PULSE-BOX LOAD, fig. 5, NOMINAL 100 mA/in.^{2} CELL CURRENT DENSITY)

Battery designation	Ambient temperature (C)	Battery internal resistance (ohms at 15 s)	Battery internal resistance (ohms at 165 s)	Remarks
WE-70	+60	--	4.08(189 s)	--
WE-71	+60	--	4.27	--
WE-80	+60	1.29	3.63	Pulsed every 15 s
WE-87	+60	--	3.09	--
WE-99	+60	--	4.04	--
WE-108	+60	--	4.67	--
WE-122	+60	--	5.05	--
WE-128	+60	--	5.05	--
WE-136	+60	0.806	3.96	Pulsed every 15 s
WE-142	+60	--	4.86	--
WE-155	+60	--	6.00	--
WE-178	+60	--	5.48	--
WE-198	+60	0.901	4.76	Pulsed every 15 s
WE-205	+60	--	5.48	--
WE-206	+60	--	--	Not pulsed
WE-208	+60	--	--	Not pulsed
WE-138	+25	--	3.40	--
WE-139	+25	0.667	3.61	Pulsed every 15 s
WE-162	+25	0.889 (10 s)	3.40	Pulsed every 15 s
WE-170	+25	--	--	Open circuit first 205 s
WE-186	+29	--	3.76	--
WE-72	-40	--	--	No pulse function
WE-76	-40	--	7.45	--
WE-89	-40	--	6.71	--
WE-95	-40	--	8.07	--
WE-102	-32	1.08	8.71	Pulsed every 15 s
WE-121	-32	--	9.56	--
WE-151	-32	--	9.62	--
WE-159	-32	--	4.88 (187 s)	--
WE-160	-32	--	10.08	--
WE-176	-32	--	10.00	--
WE-193	-32	--	9.83	--
WE-209	-32	--	10.91	--
WE-210	-32	--	8.86	--
		Average battery internal resistance at 165 s		
	+60 C	4.60 ± 0.80 ohm	(0.80 = σ_{n-1})	
	+25 C	3.54 ± 0.18 ohm	(0.18 = σ_{n-1})	
	-40 C	8.72 ± 1.70 ohm	(1.70 = σ_{n-1})	

applied and recovered quickly (1 to 2 ms) when the pulse loads were removed. During testing, the current pulses were usually applied 165 s after activation in order to test pulse capability under the worst conditions. The pulses did not significantly affect battery life to 18 V under the 184-ohm load regardless of when or if they were applied. The measurements were made every 15 s for some batteries (table 7), and even this did not affect battery life to 18 V significantly. The internal resistances plotted versus time are shown in figure 8.

The electrical performance of the PS132 final-design batteries is shown in table 8. A total of 140 batteries was built and, of these, 34 randomly selected batteries were tested at HDL over the required temperature range of -40 to +140 F (-40 to +60 C). All these batteries met all the requirements, and no difficulties of any kind were observed.

A total of 83 randomly selected PS132 final-design batteries was supplied to the Navy by April 1978. No failures or difficulties were noted by the Navy during bench and in-flight testing. The remainder of the 140 final-design batteries was stored at HDL for further test and evaluation.

TABLE 7. INTERNAL PS132 FINAL-DESIGN BATTERY RESISTANCE VERSUS DISCHARGE TIME (PULSE-BOX LOAD, fig. 5, NOMINAL 100 mA/in.^{2} CELL CURRENT DENSITY)

Time (s)	Battery internal resistance (ohms)			
	WE-80 (60 C)	WE-136 (60 C)	WE-139 (25 C)	WE-102 (-32 C)
15	1.29	0.806	0.667	1.08
30	1.09	1.18	0.743	1.11
45	1.29	1.21	0.971	1.17
60	1.29	1.27	1.18	1.28
75	1.70	1.30	1.25	1.52
90	2.14	1.48	1.45	1.87
105	2.56	1.83	1.77	2.45
120	2.88	2.32	2.18	3.29
135	3.20	2.85	2.73	4.68
150	3.36	3.32	3.25	6.82
165	3.63	3.96	3.61	8.71
180	4.23	4.36	3.86	11.4
195	5.13	4.76	4.53	15.8

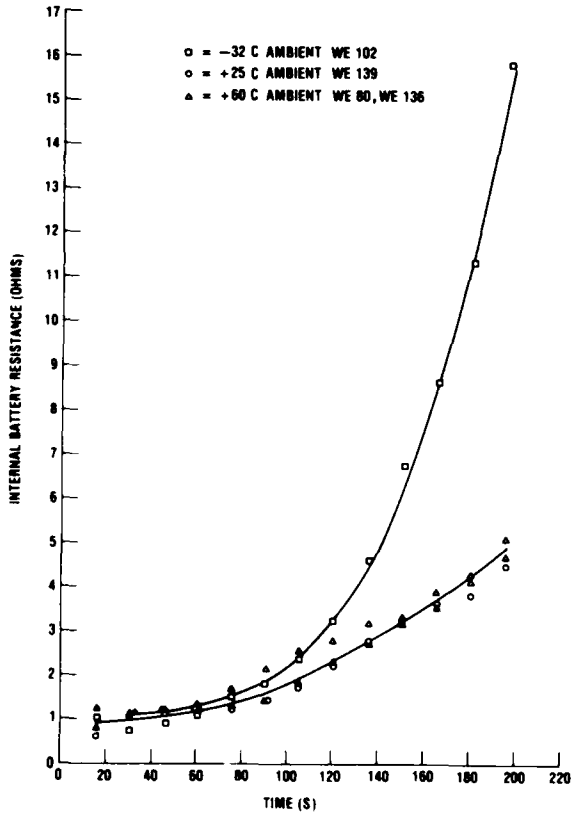

Figure 8. Internal PS132 thermal battery resistance versus discharge time.

TABLE 8. ELECTRICAL PERFORMANCE OF PS132 FINAL-DESIGN BATTERIES (PULSE-BOX LOAD, fig. 5 NOMINAL 100-mA/in.^{2} CELL CURRENT DENSITY)

Battery designation[a]	Ambient temperature (C)	Ignition method	Rise time to 18 V (ms)	Life to 18 V (s)	Remarks
WE-70[b]	+60	Electrical	175	302	--
WE-71	+60	White starter	150	273	--
WE-80	+60	White starter	165	268	Pulsed every 15 s
WE-87	+60	Electrical	--	302	Equipment malfunction--activation data not obtained
WE-99	+60	White starter	180	248	--
WE-108	+60	Electrical	210	286	--
WE-122	+60	Electrical	170	290	--
WE-128	+60	Electrical	170	276	--
WE-136	+60	Electrical	215	289	Pulsed every 15 s
WE-142	+60	Electrical	170	303	--
WE-155	+60	Electrical	200	289	--
WE-178	+60	White starter	160	264	--
WE-198	+60	White starter	155	275	Pulsed every 15 s
WE-205	+60	White starter	160	264	--
WE-206	+60	Electrical	155	275	Not pulsed
WE-208	+60	Electrical	200	266	Not pulsed
WE-138	+25	Electrical	230	231	--
WE-139	+25	Electrical	210	235	Pulsed every 15 s
WE-162	+25	White starter	190	239	Pulsed every 15 s
WE-170	+25	White starter	--	282	Equipment malfunction--open circuit first 205 s
WE-186	+29	White starter	180	268	--
WE-72	-40	Electrical	--	179	Leads reversed in test fixture: rise time data lost
WE-76	-40	Electrical	203	180	--
WE-89	-40	Electrical	190	179	--
WE-95	-40	Electrical	255	173	--
WE-102	-32	White starter	200	175	Pulsed every 15 s
WE-121	-32	White starter	200	183	--
WE-151	-32	Electrical	210	174	--
WE-159	-32	Electrical	220	210	--
WE-160	-32	Electrical	240	173	--
WE-176	-32	White starter	195	165	--
WE-193	-32	White starter	195	173	--
WE-209	-32	White starter	185	165	--
WE-210	-32	White starter	190	175	--
			Average battery lifetimes		
	+60 C	279 ± 16 s		16 = σ_{n-1}	
	+25 C	251 ± 23 s		23 = σ_{n-1}	
	-40 C	177 ± 11 s		11 = σ_{n-1}	

[a] Sixty-nine batteries built before design was finalized.
[b] No electrical noise or battery difficulty in any test.

4. SUMMARY AND CONCLUSIONS

The PS132 thermal battery was developed at HDL and is one of the smallest batteries of its kind capable of meeting its current, voltage, and lifetime requirements. The PS132 uses the Ca/LiCl-KCl eutectic-SiO_2/$CaCrO_4$ electrochemical system with pressed pellet technology.[1] Thirty-four PS132 final-design batteries were tested at HDL, 83 were supplied to the Navy, and 23 remain at HDL for future testing. Although the task originally called for 110 batteries to be delivered by December 1977, the delivery of 83 units in April 1978 was acceptable to the Navy. In-flight testing of the final-design batteries was done by NSWC Dahlgren. No battery failure or difficulty was observed in any of the final-design batteries that were tested.

A comprehensive HDL development program (400 batteries built and tested) showed that processing the DEB powder used in the PS132 was the major difficulty. PS132 batteries fabricated using most commercial DEB powders generated internal electrical short circuits during operation, as shown in figure 2. These short circuits were caused by the formation of excessive amounts of $CaLi_2$ molten metal in the electrochemical cells. The processing of DEB powder to avoid these short circuits in the PS132 is more difficult than for most thermal batteries because of the PS132's space and performance requirements. Only one batch of five commercial DEB powder batches tested proved acceptable for use in the PS132. The construction of a large number of successful batteries from this batch did show, however, that acceptable PS132 DEB powder can be made by commercial processing methods.

The gas atmosphere inside a sealed PS132 thermal battery was found to affect both heat loss rates from the thermal cells and the chemical reactions within the thermal cells. Previous work showed that hydrogen gas is expelled from the pyrotechnic materials used to heat the thermal cells when the battery is activated.[11] This hydrogen gas has a high thermal conductivity and can increase the heat loss rate from the thermal cells markedly,[12] as was confirmed experimentally for the PS132. The hydrogen gas may also react chemically with the $CaCrO_4$ depolarizer because sealed thermal batteries showed a green color for the DEB pellet (Cr_2O_3) while unsealed batteries discharged under identical conditions showed the original yellow color of $CaCrO_4$ after firing. Water vapor is also known to be expelled from heated pyrotechnic materials,[11] and it is believed that water vapor reacting with the pure calcium anode and/or with the $CaLi_2$ molten metal is responsible for the observed reduction of $CaLi_2$ molten metal formation in sealed PS132 batteries.

There is reason to believe that the one definitely acceptable commercial DEB powder batch had been water contaminated because it had been in storage under high humidity, sealed only with a metal screw-type lid and cardboard liner. Furthermore, it was shown that the DEB powder from the top of the jar

---

[1] D. Bush, A Sixty-Minute Thermal Battery, Sandia Laboratories, Albuquerque, NM, SAND 75-0454 (March 1976).

[11] F. Bachner and C. Alexander, Techniques for Measuring Gas Evolved During Combustion of Pyrotechnic Heat Powders, Harry Diamond Laboratories, HDL-TM-68-4 (February 1968).

[12] F. Krieger, Fusible Heat Reservoirs for Thermal Batteries, 26th Power Sources Symposium, PSC Publications Committee, Red Bank, NJ (May 1974), 129.

near the lid was far superior in battery performance to DEB powder from farther down in the jar. A preliminary DTA (differential thermal analysis) of the successful commercial DEB powder showed no measurable water evolution at temperatures from 25 to 400 C. However, the amount of water present in DEB powder is known to be small, and the water is subject to hydrolytic decomposition.[13] It appears that cyclic reactions may occur between H_2, H_2O, and heated components of the battery so that a small quantity of water vapor or hydroxyl ion in the DEB powder may greatly reduce $CaLi_2$ molten metal formation. Further efforts to measure the water or hydroxyl ion content of DEB powder are in progress.

One of the major problems with processing DEB powder at the present time is that there is no definitive test for DEB powder quality. Presently, the only reliable method of testing DEB powder is to build the powder into a thermal battery and observe the resultant battery performance. This method is expensive and time-consuming. In addition, results may be confounded by battery failures that may result from factors other than DEB powder processing. Because much information on the PS132 operation is available from the development program, and because it is more difficult to make successful DEB powder for the PS132 than for most thermal batteries, proper performance of a DEB powder batch in the PS132 should be an instructive criterion in a DEB powder processing study.

---

[13] H. Laitinen, W. Ferguson, and R. Osteryoung, Preparation of Pure Fused Lithium Chloride-Potassium Chloride Eutectic Solvent, J. Electrochem. Soc., 104 (August 1957), 516.

LITERATURE CITED

(1) D. Bush, A Sixty-Minute Thermal Battery, Sandia Laboratories, Albuquerque, NM, SAND 75-0454 (March 1976).

(2) M. Templeman, Thermal Battery Discharge Characteristics, United States Naval Ordnance Laboratory, White Oak, MD, NOLTR 64-14 (February 1966).

(3) C. Lofton et al, A Chemical and Physical Characterization of Calcium and Barium Chromates and Thermal Cell Performance of Calcium Chromates, Air Force Aeropropulsion Laboratory, Air Force Wright Aeronautical Laboratories, Wright Patterson Air Force Base, OH, AFAPL-TR-76-85 (April 1977).

(4) D. Bush, Electrolyte-Binder Powder Fusing Study, Sandia Laboratories, Albuquerque, NM, SC-TM-72-0651 (October 1972).

(5) R. Clark, Heat of Reaction Determinations in the System Ca-LiCl-KCl-$CaCrO_4$-SiO_2 Using Differential Scanning Calorimetry, Thermochim. Acta, 26 (1978), 49.

(6) R. Walton, A Chemical and Physical Characterization of Calcium and Barium Chromates and Thermal Cell Performance of Calcium Chromates, Air Force Aeropropulsion Laboratory, Air Force Wright Aeronautical Laboratories, Wright Patterson Air Force Base, OH, AFAPL-TR-79-2089 (November 1979).

(7) D. Bush, Thermal Battery, U.S. Patent 3,885,989 (27 May 1975).

(8) A. Baldwin, A Long-Life, Low Voltage, Power Thermal Battery, 26th Power Sources Symposium, PSC Publications Committee, Red Bank, NJ (1974), 137.

(9) R. Clark and K. Grothaus, Thermal Battery Having Protectively Coated Calcium Anode to Prevent Alloy Shorting, U.S. Patent 3,527,615 (8 September 1975).

(10) D. Bush, Thermal Battery, U.S. Patent 3,898,101 (5 August 1975).

(11) F. Bachner and C. Alexander, Techniques for Measuring Gas Evolved During Combustion of Pyrotechnic Heat Powders, Harry Diamond Laboratories, HDL-TM-68-4 (February 1968).

(12) F. Krieger, Fusible Heat Reservoirs for Thermal Batteries, 26th Power Sources Symposium, PSC Publications Committee, Red Bank, NJ (May 1974), 129.

(13) H. Laitinen, W. Ferguson, and R. Osteryoung, Preparation of Pure Fused Lithium Chloride-Potassium Chloride Eutectic Solvent, J. Electrochem. Soc., 104 (August 1957), 516.

APPENDIX A.--HEAT-TRANSFER ANALYSIS OF THE PS132 THERMAL BATTERY

CONTENTS

Page

A-1. INTRODUCTION 31

A-2. ANALYSIS OF COPPER/HEAT-PELLET STACK HEAT-TRANSFER 33

A-3. PS132 PROTOTYPE FORERUNNER HEAT-TRANSFER ANALYSIS 38

A-4. CONCLUSIONS 43

LITERATURE CITED 44

FIGURES

A-1. Natural logarithm of temperature difference ($T - T_o$) versus time for the copper/heat-pellet stack configuration 36

A-2. Natural logarithm of temperature difference ($T - T_o$) versus time for the PS132 prototype forerunner battery S-43 during battery operation 40

A-3. Natural logarithm of temperature difference ($T - T_o$) versus time for the PS132 prototype forerunner battery S-43 below the electrolyte freezing point 43

TABLES

A-1. Copper/Heat-Pellet Stack Configuration 31

A-2. Temperature-Time Behavior of Copper/Heat-Pellet Configuration 33

A-3. Heat Capacity of Copper/Heat-Pellet Stack Configuration 34

A-4. Geometric Shape Factor for Copper/Heat-Pellet Stack Configuration 37

A-5. Temperature-Time Behavior of PS132 Prototype Forerunner Battery (Battery S-43) During Battery Operation 38

A-6. Heat Capacity of PS132 Prototype Forerunner Battery (Battery S-43) (370 to 520 C) 39

A-7. Geometric Shape Factor for PS132 Prototype Forerunner Battery (Battery S-43) 41

A-8. Temperature-Time Behavior of PS132 Prototype Forerunner Battery (Battery S-43) Below the Electrolyte Freezing Point 42

APPENDIX A.--HEAT-TRANSFER ANALYSIS OF THE PS132 THERMAL BATTERY

A-1. INTRODUCTION

Calculations[1] showed that conduction was the major mode of heat loss in the PS132. Radiation and convection heat losses were negligibly small by comparison. To examine the conduction mode of heat loss in more detail, two experiments were performed. In the first experiment, a copper/heat-pellet stack similar in geometry to the PS132 was used (table A-1). The heat capacity of the copper/heat-pellet stack can be well-specified, and no heat-generating reactions occur in the copper/heat-pellet stack, so this method is quite appropriate for a beginning heat-transfer analysis. The second experiment was done with the PS132 prototype forerunner battery S-43 (see main body of report--table 1, fig. 3 and 4, and sect. 2). These experiments were intended to confirm the effect of gases expelled from the heated battery components on battery operation. The experiments also showed that exothermic chemical reactions occur during battery operation. The heat-transfer analyses were done from the cooling curves of the units as discussed below.

TABLE A-1. COPPER/HEAT-PELLET STACK CONFIGURATION

Component	Diameter (in.)		Thickness (in.)	Mass (g)
	Outer	Inner		
Two bottom asbestos disks	1.50	--	0.063	1.532
Three asbestos rings	1.25	0.468	0.092	1.274
Half Fiberfrax ring	1.25	0.468	0.018	0.157
Insulation heat pellet	1.25	0.442	0.063	4.544
Half Fiberfrax ring	1.25	0.468	0.018	0.167
Three asbestos rings	1.25	0.468	0.093	1.354
Half Fiberfrax ring	1.25	0.468	0.018	0.131
Heat pellet	1.25	0.442	0.032	2.317
Seven copper rings	1.25	0.468	0.063	8.934
Heat pellet	1.25	0.442	0.032	2.323
Seven copper rings	1.25	0.468	0.066	9.260
Heat pellet	1.25	0.442	0.032	2.331
Four copper rings	1.25	0.468	0.036	5.231
Nickel thermocouple ring	1.25	0.468	0.005	0.756
Three copper rings	1.25	0.468	0.027	3.923
Heat pellet	1.25	0.442	0.032	2.322
Seven copper rings	1.25	0.468	0.059	8.555
Heat pellet	1.25	0.442	0.032	2.321
Seven copper rings	1.25	0.468	0.066	9.787
Heat pellet	1.25	0.442	0.032	2.330
Seven copper rings	1.25	0.468	0.066	9.451
Nickel thermocouple ring	1.25	0.468	0.005	0.755
Heat pellet	1.25	0.442	0.032	2.311

[1] F. Krieger and R. Comyn, Fusible Thermostat for Thermal Power Supplies, Harry Diamond Laboratories, HDL-TR-1644 (November 1973).

APPENDIX A

TABLE A-1. COPPER/HEAT-PELLET STACK CONFIGURATION (Cont'd)

Component	Diameter (in.)		Thickness (in.)	Mass (g)
	Outer	Inner		
Half Fiberfrax ring	1.25	0.468	0.018	0.174
Three asbestos rings	1.25	0.468	0.090	1.286
Half Fiberfrax ring	1.25	0.468	0.018	0.140
Insulation heat pellet	1.25	0.442	0.067	5.013
Half Fiberfrax ring	1.25	0.468	0.018	0.185
One asbestos ring	1.25	0.468	0.029	0.405
Two thin asbestos rings	1.25	0.468	0.014	0.162
One asbestos ring	0.984	0.468	0.032	0.254
Two top asbestos disks	0.984	--	0.059	0.637
Two Fiberfrax side wraps	--	--	--	2.819
Heat paper fuse train	--	--	--	0.948
Asbestos center wrap	--	--	--	0.395
White starter	--	--	--	6.410

If heat is lost by conduction only, Newton's law of cooling holds. That is,

$$\frac{dq}{dt} = -\zeta\left(T - T_o\right) \qquad \text{(A-1)}$$

or

$$\left(\Sigma_i M_i C_i\right) \frac{dT}{dt} = -\zeta\left(T - T_o\right) \ , \qquad \text{(A-2)}$$

where

q = heat loss (cal),

t = time (s),

dq/dt = heat-loss rate (cal/s),

ζ = constant (cal/s-C),

T = temperature of cooling mass (C),

T_o = temperature of battery case (C),

M_i = mass of i^{th} component of cooling mass (g),

C_i = specific heat of i^{th} component of cooling mass (cal/g-C),

$\left(\Sigma_i M_i C_i\right)$ = heat capacity of cooling mass (cal/C), and

$\frac{dT}{dt}$ = cooling rate (C/s).

From equation (A-2),

$$\frac{dT}{T - T_o} = - \frac{\zeta dt}{\left(\Sigma_i M_i C_i\right)} \quad .$$

By integration,

$$\ell n\left(T - T_o\right) = - \frac{\zeta t}{\left(\Sigma_i M_i C_i\right)} + \text{constant} \quad . \qquad \text{(A-3)}$$

From equation (A-3), the slope of the plot of $\ln(T - T_o)$ versus t is equal to $-\zeta/\left(\Sigma_i M_i C_i\right)$. Multiplication of this slope by $\left(\Sigma_i M_i C_i\right)$ determines the constant ζ. The constant ζ is then multiplied by the temperature difference $\left(T - T_o\right)$ to obtain the experimental heat-loss rate as in equation (A-1).

A-2. ANALYSIS OF COPPER/HEAT-PELLET STACK HEAT TRANSFER

The copper/heat-pellet stack was initiated at an ambient temperature of -46 C; the resulting temperature-time behavior is shown in table A-2. The heat-transfer analysis was done for the first 180 s after initiation. This corresponds to the approximate lifetime of the PS132 when fired at -40 C. By 180 s, the copper/heat-pellet stack cooled to an average temperature of 346 C, which is similar to the average stack temperature of a PS132 battery 180 s after ignition when fired at -40 C.

TABLE A-2. TEMPERATURE-TIME BEHAVIOR OF COPPER/HEAT-PELLET CONFIGURATION

Time (s)	Stack end temperature (C)	Stack center temperature (C)	Average stack temperature (C)	Case temperature (C)	Average stack-to-case temperature difference (C)
0	-46	-47	-47	-46	-1
2	477	450	464	-44	508
6	470	465	468	-37	505
15	472	466	469	-14	483
30	466	464	465	10	455
60	441	446	444	35	409
90	414	423	419	48	371
120	388	397	393	56	337
150	363	373	368	61	307
180	341	350	346	64	282

APPENDIX A

The heat capacity $(\Sigma_i M_i C_i)$ of the copper/heat-pellet stack configuration is shown in table A-3. The heat capacity was calculated from the mass of the components and from specific heat data taken from the literature.[2,3] The specific heat data for the major components of the copper/heat-pellet stack are known to better than 1 percent. Some uncertainty in the effective heat capacity of the thermal insulation during cooling results because the exact temperature distribution in the thermal insulation is not known. In table A-3 it is assumed that the insulation in the stack (i.e., the insulation between the end-stack heat pellet and the insulation heat pellet) cools at the same rate as the insulation heat pellet and the copper/heat-pellet stack. The thermal insulation external to the stack is assumed to show a linear temperature gradient to a first approximation. This means that the external insulation yields its heat of cooling half as fast as does the stack insulation, if the case temperature T_o remains constant; thus, the effective heat capacity is half as much as for the stack insulation (table A-3). If the thermal gradient in the external thermal insulation differs from linearity, the error in this calculation of the effective heat capacity will be small because the external insulation contributes less than 10 percent to the total heat capacity.

TABLE A-3. HEAT CAPACITY OF COPPER/HEAT-PELLET STACK CONFIGURATION (370 to 520 C)

Component	Mass (g)	Specific heat (cal/g-C)	Heat capacity (cal/C)
White starter	6.410	0.1015	0.6506
Heat pellets	25.812	0.1645	4.2461
Copper rings	55.141	0.1015	5.5968
Nickel rings	1.511	0.1243	0.1878
Heat paper	0.948	0.14	0.1327
Insulation (stack)	3.647	0.25	0.9118
Insulation (external)	7.425	0.125	0.9281
			12.6539

The heat capacity shown in table A-3 can be confirmed experimentally from the measured peak temperature. For this calculation it is assumed that the external insulation is heated uniformly to the same temperature as the stack insulation during the rapid heat-transfer stage that occurs for a few seconds after ignition.[4] The total heat capacity of the copper/heat-pellet stack is then 12.6539 + 0.9281 = 13.5820 cal/C (table A-3). The heat pellets

[2] K. K. Kelley, Contributions to the Data on Theoretical Metallurgy, XIII, High Temperature Heat Content, Heat Capacity, and Entropy Data for the Elements and Inorganic Compounds, (U.S. Bureau of Mines Bulletin 584, U.S. Government Printing Office, Washington, D.C. (1960)).

[3] J. H. Perry, Chemical Engineers Handbook, 3rd ed, 3rd impression, McGraw Hill Book Company, Inc., New York (1950).

[4] M. Jakob and G. Hawkins, Elements of Heat Transfer, 3rd ed, John Wiley & Sons, Inc., New York (1957).

in the copper/heat-pellet stack were all made from 86/14 Fe/$KClO_4$ pyrotechnic powder that supplied 258 cal/g, and the heat paper supplied 400 cal/g, so the total heat supplied was 258 cal/g × 25.8 2 g + 0.948 g × 400 cal/g = 7038.7 cal. The calculated temperature rise on ignition is then 7038.7 cal ÷ 13.582 cal/C = 518 C, and the calculated peak temperature when fired at -46 C is 472 C. This compares well with the measured average stack peak temperature of 469 C in table A-2.

It should be emphasized that the heat capacity calculated in table A-3 is the average heat capacity between 370 and 520 C (the approximate operating temperature range of the PS132 thermal cells when fired at -40 C). The heat capacity from -40 to 520 C is approximately 5 percent less than the table A-3 value. Because measurement of heat capacity by this method is accurate only to approximately 10 percent, the table A-3 values were used without correction.

The linear relationship for the natural logarithm of the temperature difference ($T - T_o$) versus time for the copper/heat-pellet stack is shown in figure A-1. A least-squares fit of the data points showed a slope of $-0.003349\ s^{-1}$ and a correlation coefficient of 0.9987. The heat-loss rate is calculated from the slope:

$$\text{slope} = -0.003349\ s^{-1} = -\zeta/\Sigma_i M_i C_i$$

$$\zeta = 0.003349 \times \Sigma_i M_i C_i$$

$$= 0.003349 \times 12.65 \text{ (table A-3)}$$

$$= 0.04236 \text{ cal/s-C} \quad .$$

Then from equation (1)

$$dq/dt = -\zeta(T - T_o)$$

$$= -\ 0.04236(465 - 10)$$

$$= -19.27 \text{ cal/s} \quad .$$

This is the experimental heat-loss rate from the copper/heat-pellet stack 30 s after ignition at a temperature of 465 C, with the case temperature at 10 C. The heat-loss rate dq/dt can also be calculated using equation (A-4).[4]

$$dq/dt = KS\Delta T \quad , \qquad \text{(A-4)}$$

[4] M. Jakob and G. Hawkins, Elements of Heat Transfer, 3rd ed, John Wiley & Sons, Inc., New York (1957).

where

K = thermal conductivity of thermal insulation (cal/s-cm-C),

S = geometric shape factor (cm), and

ΔT = temperature difference (C).

The geometric shape factor for the copper/heat-pellet stack was calculated to be 130.800 cm (table A-4). The experimental insulation thermal conductivity may now be calculated from equation (A-4), using the experimental heat-loss rate:

$$K = \frac{dq/dt}{S\Delta T} = \frac{19.27 \text{ cal/s}}{130.8 \text{ cm}(465 \text{ C} - 10 \text{ C})} \approx 3.238 \times 10^{-4} \text{ cal/s-cm-C} \quad .$$

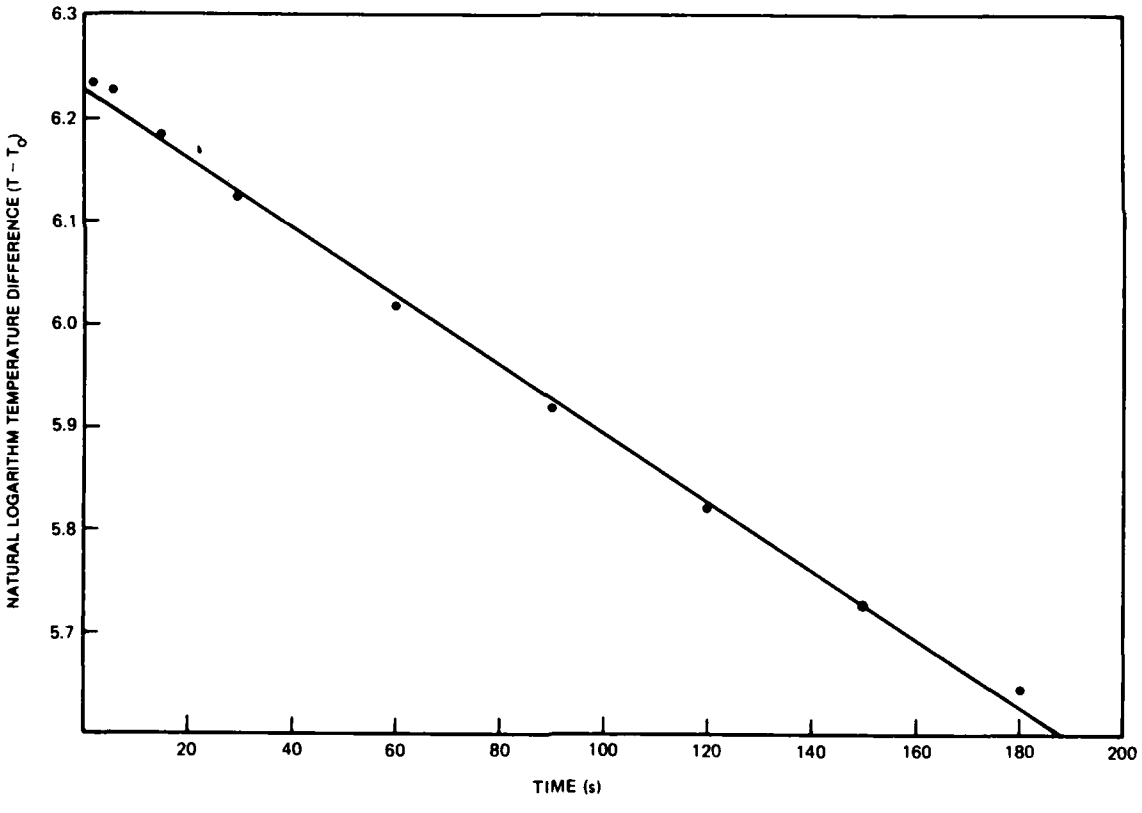

Figure A-1. Natural logarithm of temperature difference ($T - T_o$) versus time for the copper/heat-pellet stack configuration.

TABLE A-4. GEOMETRIC SHAPE FACTOR FOR COPPER/HEAT-PELLET STACK CONFIGURATION

Component	Component thickness (in.)
Insulation heat pellet	0.063
Asbestos plus Fiberfrax (compressed)	0.090
Seven stack heat pellets	0.224
Forty-two copper rings	0.383
Two nickel thermocouple rings	0.010
Asbestos plus Fiberfrax (compressed)	0.090
Insulation heat pellet	0.067
Total	0.927

$L_1 = 0.927$ in. $= 2.355$ cm $\qquad L_2 = 1.189$ in. $= 3.020$ cm

$D_1 = 1.25$ in. $= 3.175$ cm $\qquad D_2 = 1.562$ in. $= 3.967$ cm

$$S_{side} = \frac{2\pi L_1}{\ell n D_2/D_1} = \frac{(6.28319)(2.355)(1.009)}{\ell n\ (3.967/(3.175 \times 1.009))} = \frac{14.930}{0.21374} = 69.851 \text{ cm}$$

$$S_{ends} = \frac{\pi D_1^2}{L_2 - L_1} = \frac{(3.14159)(3.175 \times 1.009)^2}{3.020 - 2.355 \times 1.009} = \frac{32.242}{0.64381} = 50.080 \text{ cm}$$

$$S_{edges} = 0.54 \times 2\pi D_1 = 0.54(6.28319)(3.175)(1.009) = 10.869 \text{ cm}$$

$$S_{total} = 130.800 \text{ cm}$$

0.54 = empirical factor[a]

1.009 = expansion factor for inner cylinder on heating[b]

[a] M. Jakob and G. Hawkins, Elements of Heat Transfer, 3rd ed, John Wiley & Sons, Inc., New York (1957).

[b] J. H. Perry, Chemical Engineers Handbook, 3rd ed., 3rd impression, McGraw Hill Book Company, Inc., New York (1950).

The thermal conductivity of the asbestos in a nitrogen atmosphere was measured in a separate (steady-state) experiment (eq A-5). The equation (A-5) values are also correct for asbestos in an air atmosphere because the thermal conductivities of nitrogen and air are equal within 2 percent at the temperatures of interest:

$$K = 1.06 \times 10^{-4} + 2.00 \times 10^{-7}\ T_m \text{ cal/s-cm-C} \quad , \qquad \text{(A-5)}$$

where

T_m = median insulation temperature. When T = 465 and T_o = 10 as above:

$$T_m = {}^1/_2(T + T_o) = 237.5 \text{ C} ,$$

$$K = 1.06 \times 10^{-4} + 2.0 \times 10^{-7} \times 237.5 = 1.535 \times 10^{-4} \text{ cal/s-cm-C} .$$

The manufacturer of Fiberfrax reports its thermal conductivity to be 1.701×10^{-4} cal/s-cm-C at 237.5 C. The asbestos and Fiberfrax thermal conductivities are therefore equal to less than 11 percent. The measured thermal conductivity of the asbestos and Fiberfrax from the copper/heat-pellet stack cooling curves is more than twice the thermal conductivity of the asbestos in air ($3.238 \times 10^{-4}/1.535 \times 10^{-4} = 2.109$). This shows that the porous asbestos and Fiberfrax thermal insulation have been contaminated with high-thermal conductivity hydrogen gas.[1,5]

A-3. PS132 PROTOTYPE FORERUNNER HEAT-TRANSFER ANALYSIS

The heat-transfer analysis of section A-2 was applied to the PS132 prototype forerunner battery S-43 (see body of report, table 1, for construction, and fig. 3, 4). The temperature-time behavior immediately after ignition is shown in table A-5. Battery S-43 was fired at high ambient temperature (+62 C). A heat-transfer analysis was then done for the first 180 s after activation to confirm the presence of exothermic chemical reactions during battery operation. A second heat-transfer analysis after the electrolyte was frozen (from 420 to 780 s after activation) confirmed the presence of hydrogen gas in the porous thermal insulation.

TABLE A-5. TEMPERATURE-TIME BEHAVIOR OF PS132 PROTOTYPE FORERUNNER BATTERY (BATTERY S-43) DURING BATTERY OPERATION

Time (s)	Stack end temperature (C)	Stack center temperature (C)	Average stack temperature (C)	Case temperature (C)	Average stack-to-case temperature difference (C)
0	62	62	62	62	0
2	561	503	532	69	463
6	605	546	576	82	494
15	631	561	596	101	495
30	624	582	603	117	486
45	607	603	605	130	475
60	591	614	603	141	462
90	561	620	591	163	428
120	534	604	569	180	389
150	508	576	542	193	349
180	480	534	507	200	307

[1] F. Krieger and R. Comyn, Fusible Thermostat for Thermal Power Supplies, Harry Diamond Laboratories, HDL-TR-1644 (November 1973).

[5] R. McIntyre, Procedure for Determination of Gas Evolved by Thermite Mixtures, Diamond Ordnance Fuze Laboratories, TR-702 (February 1960).

The heat capacity of battery S-43 is shown in table A-6. The specific heat data are believed correct to within about 5 percent. The heat capacity data can be confirmed experimentally, as was done in section A-2 for the copper/heat-pellet stack. For battery S-43, the 10 stack heat pellets (table 1, body of report) were of mass 11.643 g and were made from 88/12 Fe/$KClO_4$ pyrotechnic powder with a heat output of 221 cal/g. The two insulation heat pellets were of mass 9.146 g and were made from 86/14 Fe/$KClO_4$ pyrotechnic powder with a heat output of 258 cal/g. The specific heats of the 88/12 and 86/14 Fe/$KClO_4$ heat-pellet ashes are equal within 5 percent, and this difference has been neglected in table A-6. The heat-paper heat output was 400 cal/g. The total amount of heat evolved from all the pyrotechnic materials is therefore 221 cal/g × 11.643 g + 258 cal/g × 9.146 g + 0.854 g × 400 cal/g = 5274.4 cal (table A-6). The calculated temperature rise (table A-6) is 5274.4 cal/(9.2990 + 1.0013) = 512 C. The measured temperature rise 15 s after activation in table A-5 is 596 C - 62 C = 534 C, and is within 5 percent of the calculated value. Unlike the copper/heat-pellet stack, the average temperature of the battery S-43 stack continued to increase after 15 s following initiation because of chemical side reactions in the S-43 electrochemical cells (table A-5, fig. 3 and 4, body of report).

TABLE A-6. HEAT CAPACITY OF PS132 PROTOTYPE FORERUNNER BATTERY (S-43) (370 to 520 C)

Component	Mass (g)	Specific heat (cal/g-C)	Heat capacity (cal/C)
White starter	6.483	0.1015	0.6580
Heat pellets (86/14)	9.146	0.1645	1.5045
Heat pellets (88/12)	11.643	0.1645	1.9153
Bimetal anodes (iron)	6.116	0.1508	0.9223
Bimetal anodes (calcium)	1.738	0.1915	0.3328
Nickel rings	3.030	0.1243	0.3766
DEB pellets	7.236	0.2488	1.8003
Heat paper	0.854	0.14	0.1196
Insulation (stack)	2.673	0.25	0.6683
Insulation (external)	8.010	0.125	1.0013
		Total	9.2990

The natural logarithm of temperature difference ($T - T_o$) versus time for battery S-43 during the first 180 s after activation is shown in figure A-2. A least-squares fit of the data points showed a slope of -0.002498 s^{-1} and a correlation coefficient of 0.9570. The poor correlation was caused by the convex shape of the curve as a result of the chemical exotherms. The heat-loss rate was calculated from the slope as before. From equation (A-3),

APPENDIX A

$$\text{slope} = \frac{-\zeta}{\Sigma_i (M_i C_i)} = -0.002498 \text{ s}^{-1},$$

$$\zeta = 0.002498 \times \Sigma_i M_i C_i$$

$$= 0.002498 \times 9.2990 \text{ (table A-6)}$$

$$= 0.02323 \text{ cal/s-C} \quad .$$

Then from equation (A-1),

$$dq/dt = -\zeta(T - T_o) = - 0.02323(596 - 101)$$
$$= -11.50 \text{ cal/s} \quad .$$

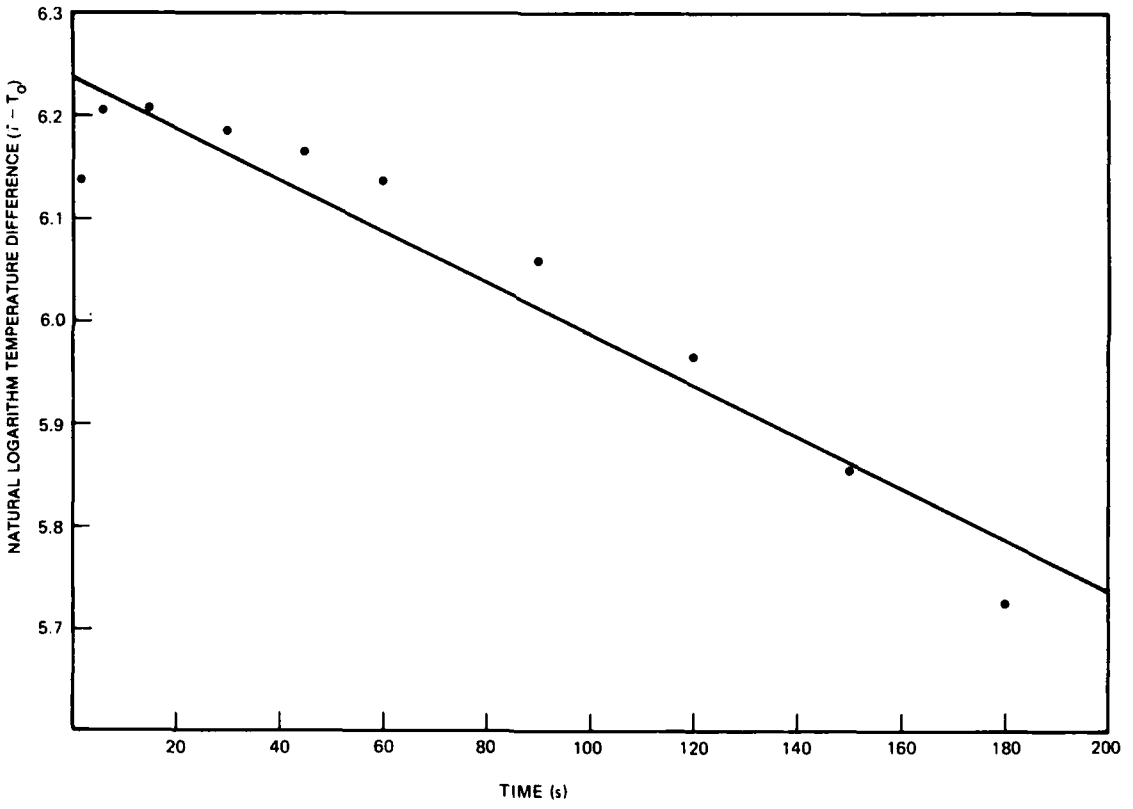

Figure A-2. Natural logarithm of temperature difference ($T - T_o$) versus time for the PS132 prototype forerunner battery S-43 during battery operation.

This is the experimental heat-loss rate 15 s after initiation, with the battery stack at an average temperature of 596 C and the case temperature at 101 C. The thermal conductivity is now calculated from equation (A-4) as in section A-2 using the geometric shape factor for battery S-43 calculated in table A-7.

$$K = \frac{dq/dt}{S\Delta T} = \frac{11.50}{114.654(596 - 101)} = 2.026 \times 10^{-4} \text{ cal/s-cm-C} \quad .$$

TABLE A-7. GEOMETRIC SHAPE FACTOR FOR PS132 PROTOTYPE FORERUNNER BATTERY (BATTERY S-43)

Component	Component thickness (in.)
Insulation heat pellet	0.065
Asbestos plus Fiberfrax (compressed)	0.060
Ten stack heat pellets	0.166
Nine bimetal rings	0.127
Nine DEB pellets	0.270
Two nickel current collectors	0.010
Two nickel thermocouple rings	0.010
Asbestos plus Fiberfrax (compressed)	0.060
Insulation heat pellet	0.065
Total	0.833

L_1 = 0.833 in. = 2.116 cm $\qquad$ L_2 = 1.150 in. = 2.921 cm

D_1 = 1.25 in. = 3.175 cm $\qquad$ D_2 = 1.562 in. = 3.967 cm

$$S_{side} = \frac{2\pi L_1}{\ell n\, D_2/D_1} = \frac{(6.28319)(2.116)(1.009)}{\ell n(3.967/(3.175 \times (1.009))} = \frac{13.415}{0.21374} = 62.763 \text{ cm}$$

$$S_{ends} = \frac{\pi D_1^2}{L_2 - L_1} = \frac{(3.14159)\ (3.175 \times 1.009)^2}{2.921 - 2.116 \times 1.009} = \frac{32.242}{0.78596} = 41.022 \text{ cm}$$

$$S_{edges} = 0.54 \times 2\pi D_1 = 0.54(6.28319)(3.175)(1.009) = 10.869 \text{ cm}$$

$$S_{total} = 114.654 \text{ cm}$$

0.54 = empirical factor[a]

1.009 = expansion factor for inner cylinder on heating[b]

[a] M. Jakob and G. Hawkins, Elements of Heat Transfer, 3rd ed, John Wiley & Sons, Inc., New York (1957).

[b] J. H. Perry, Chemical Engineers Handbook, 3rd ed., 3rd impression, McGraw Hill Book Company, Inc., New York (1950).

APPENDIX A

The thermal conductivity of asbestos in an air atmosphere is again calculated from equation (A-5):

$$T_m = \frac{T + T_o}{2} = \frac{596 + 101}{2} = 349 \text{ C},$$

$$K = 1.06 \times 10^{-4} + 2.00 \times 10^{-7} \times 349 = 1.758 \times 10^{-4} \text{ cal/s-cm-C} .$$

The measured thermal conductivity of the asbestos and Fiberfrax in battery S-43 during battery operation is only 15 percent greater than the thermal conductivity of asbestos in air ($[2.026 \times 10^{-4}]/[1.758 \times 10^{-4}] = 1.152$) when measured by this method. This is because of the exothermic chemical reactions that compensate for the heat loss.

The presence of hydrogen gas in the porous thermal insulation was proved by analysis of the cooling curves below the electrolyte freezing point where exothermic chemical reactions can no longer occur (table A-8, fig. A-3). The slope of the least-squares-fit line in figure A-3 is -0.003423 s^{-1}. The correlation coefficient was 0.9939, greatly improved from the 0.9570 value obtained when exothermic chemical reactions were present. By the same calculations as above, the measured heat-loss rate is 1.878 cal/s at 540 s after initiation where the average stack temperature is 217 C and the case temperature is 158 C; the measured thermal conductivity is 2.776×10^{-4} cal/s-cm-C. The thermal conductivity of asbestos in air at a mean temperature of $^1/_2(217 + 158) = 187.5$ C is 1.435×10^{-4} from equation (A-5). The measured thermal conductivity of the asbestos and Fiberfrax is nearly twice the thermal conductivity of asbestos measured in an air atmosphere ($[2.776 \times 10^{-4}]/[1.435 \times 10^{-4}] = 1.934$). This shows that the porous asbestos and Fiberfrax insulation have been contaminated with high-thermal-conductivity hydrogen gas (compare sect. A-2).

TABLE A-8. TEMPERATURE-TIME BEHAVIOR OF PS132 PROTOTYPE FORERUNNER BATTERY (BATTERY S-43) BELOW THE ELECTROLYTE FREEZING POINT

Time (s)	Stack end temperature (C)	Stack center temperature (C)	Average stack temperature (C)	Case temperature (C)	Average stack-to-case temperature difference (C)
420	281	284	283	182	101
540	215	218	217	158	59
660	176	178	177	136	41
780	150	147	149	120	29

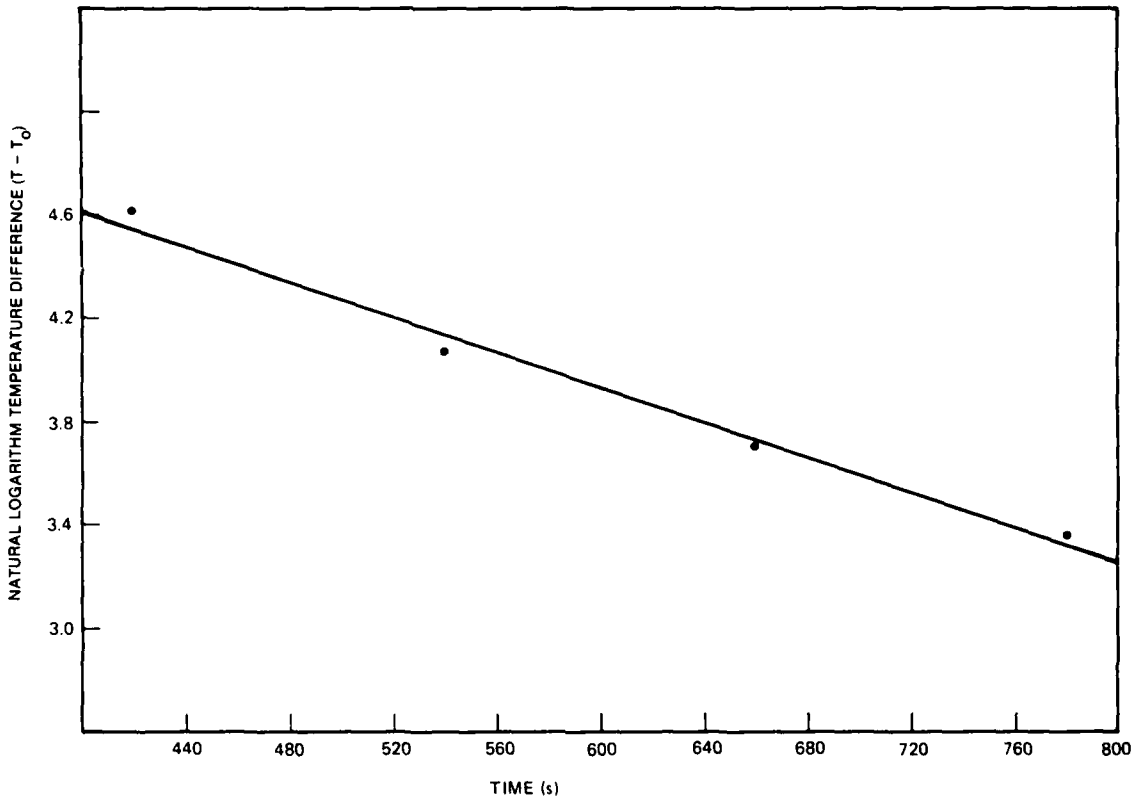

Figure A-3. Natural logarithm of temperature difference ($T - T_o$) versus time for the PS132 prototype forerunner battery S-43 below the electrolyte freezing point.

A-4. CONCLUSIONS

The measurement of thermal conductivities by the method in this appendix has been shown previously to be accurate to within ±15 percent.[1] This relatively large amount of error occurs primarily because the temperature distribution in the heated components and in the thermal insulation during cooling is not certain. The composition of the gases in the porous thermal insulation may also change during cooling.

The heat-transfer analyses, combined with the known gas evolution properties of the pyrotechnic materials used,[5] are sufficiently accurate to show that a large amount of high-thermal-conductivity hydrogen gas is present in the thermal insulation of the cooling units. This hydrogen gas can react with $CaCrO_4$ to form H_2O, and the H_2O can then react with metallic Ca or $CaLi_2$ to reduce $CaLi_2$ molten metal accumulation as discussed in section 2 of the body of the report. The heat-transfer analyses also confirm the presence of exothermic chemical reactions in the operating PS132 battery.

---

[1] F. Krieger and R. Comyn, Fusible Thermostat for Thermal Power Supplies, Harry Diamond Laboratories, HDL-TR-1644 (November 1973).

[5] R. McIntyre, Procedure for Determination of Gas Evolved by Thermite Mixtures, Diamond Ordnance Fuze Laboratories, TR-702 (February 1960).

APPENDIX A

LITERATURE CITED

(1) F. Krieger and R. Comyn, Fusible Thermostat for Thermal Power Supplies, Harry Diamond Laboratories, HDL-TR-1644 (November 1973).

(2) K. K. Kelley, Contributions to the Data on Theoretical Metallurgy, XIII, High Temperature Heat Content, Heat Capacity, and Entropy Data for the Elements and Inorganic Compounds, U.S. Bureau of Mines Bulletin 584, (U.S. Government Printing Office, Washington, D.C. (1960)).

(3) J. H. Perry, Chemical Engineers Handbook, 3rd ed, 3rd impression, McGraw Hill Book Company, Inc., New York (1950).

(4) M. Jakob and G. Hawkins, Elements of Heat Transfer, 3rd ed, John Wiley & Sons, Inc., New York (1957).

(5) R. McIntyre, Procedure for Determination of Gas Evolved by Thermite Mixtures, Diamond Ordnance Fuze Laboratories, TR-702 (February 1960).

DISTRIBUTION LIST

ADMINISTRATOR
DEFENSE TECHNICAL INFORMATION CENTER
ATTN DTIC-DDA (12 COPIES)
CAMERSON STATION, BUILDING 5
ALEXANDRIA, VA 22304-6145

COMMANDER
US ARMY MATERIEL COMMAND
5001 EISENHOWER AVE
ALEXANDRIA, VA 22333-0001

OFFICE OF THE DIRECTOR OF
DEFENSE RESEARCH & ENGINEERING
ATTN MR. THORKILDSEN
THE PENTAGON
WASHINGTON, DC 20301

DIRECTOR, ADVANCED RESEARCH
PROJECTS AGENCY
ATTN CHIEF, TECH OPERATIONS DIV
WASHINGTON, DC 20301

INSTITUTE FOR DEFENSE ANALYSIS
ATTN MR. ROBERT C. HAMILTON
400 ARMY-NAVY DRIVE
ARLINGTON, VA 22202

US DEPARTMENT OF ENERGY
ATTN MR. GEORGE B. MANNING
FE-22 (GTN)
WASHINGTON, DC 20545

US DEPARTMENT OF ENERGY
OFFICE OF SOLAR ELECTRIC TECHNOLOGIES
ATTN MR. LEONARD J. ROGERS
M.S. CE31, FORRESTAL BLDG
WASHINGTON, DC 20585

US DEPARTMENT OF ENERGY
OFFICE OF ADVANCED CONSERVATION
TECHNOLOGIES
ATTN DR. ALBERT R. LANDGREBE
ELECTROCHEMICAL RESEARCH BRANCH
ATTN DR. JAMES H. SWISHER, THERMAL
& MECH. ENERGY STORAGE DIVISION
M.S. 6B025, FORRESTAL BLDG
WASHINGTON, DC 20585

DOD PROJECT MANAGER-MOBIL
ELECTRIC POWER
ATTN DRCPM-MEP-T, MR. JOHN T. WASDI
BLDG. 2089
7500 BACKLICK ROAD
SPRINGFIELD, VA 22150

CENTRAL INTELLIGENCE AGENCY
ATTN DR. TYLER X. MAHY
WASHINGTON, DC 20505

ARRADCOM
ATTN MR. DAVID YEDWAB
TE&S BRANCH, BLDG 61S
ATTN MR. A. E. MAGISTRO
TAW LAB, BLDG 65
DOVER, NJ 07801

DIRECTOR
US ARMY BALLISTIC RESEARCH LABORATORY
ATTN DRDAR-TSB-S (STINFO)
ABERDEEN PROVING GROUND, MD 21005

COMMANDING OFFICER
AMCCOM HQ
ATTN LIBRARY
DOVER, NJ 07081

US ARMY COMBAT SURVEILLANCE & TARGET
ACQUISITION LABORATORY
ATTN DELET-DD
FT MONMOUTH, NJ 07703

COMMANDING OFFICER
US ARMY ELECTRONICS R&D LABS
ATTN LIBRARY
FT MONMOUTH, NJ 07703

US ARMY ELECTRONICS TECHNOLOGY
& DEVICES LAB
ATTN DELET-PB, MR. EDWARD REISS
FT MONMOUTH, NJ 07703

US ARMY ELECTRONICS TECHNOLOGY &
DEVICES LABORATORY
ATTN DELET-P, DR. CARL BERGER
FT MONMOUTH, NJ 07703

US ARMY FACILITIES ENGINEERING SUPPORT
AGENCY
ATTN FESA-T, MR. JOHN BOULDIN
FT BELVOIR, VA 22060

US ARMY FOREIGN SCIENCE & TECHNOLOGY
CENTER
ATTN DRXST-MT1, MR. PHILLIP GREENBAUM
ATTN DRXST-MT1, MR. JAMES D. BUSI
ATTN DRXST-MT1, MRS. JEANETTE S. STANLEY
220 SEVENTH STREET, NE
CHARLOTTESVILLE, VA 22901

DIRECTOR
US ARMY MATERIEL SYSTEMS ANALYSIS
ACTIVITY
ATTN DRXSY-MP
ABERDEEN PROVING GROUND, MD 21005

DISTRIBUTION LIST (cont'd)

DEPARTMENT OF THE ARMY
ARMY MATERIALS & MECHANICS
RESEARCH CENTER
ATTN JAMES MCCAULEY
WATERTOWN, MA 02172

COMMANDER
US ARMY MISSILE & MUNITIONS
CENTER & SCHOOL
ATTN ATSK-CTD-F
REDSTONE ARSENAL, AL 35809

REDSTONE SCIENTIFIC INFO CENTER
US ARMY MISSILE COMMAND
ATTN CHIEF, DOCUMENT SECTION
REDSTONE ARSENAL, AL 35809

US ARMY MOBILITY EQUIPMENT R&D COMMAND
ATTN DRDME-E, MR. RICHARD T. SALE
ATTN DRDME-EC, DR. JOHANN A. JOEBSTL
ATTN DRDME-ECS, MR. WALTER TASCHEK
ATTN DRDME-ECS, MR. RICHARD N. BELT
FT BELVOIR, VA 22060

COMMANDING GENERAL
US ARMY MUNITIONS COMMAND
ATTN TECHNICAL LIBRARY
DOVER, NJ 07801

OFFICE OF THE CHIEF OF RES & DEV
DEPARTMENT OF THE ARMY
ATTN DIRECTOR, ARMY RESEARCH
WASHINGTON, DC 20310

US ARMY RESEARCH OFFICE
PO BOX 12211
ATTN DR. BERNARD F. SPIELVOGEL
TRIANGLE RESEARCH PARK, NC 27709

US ARMY TANK-AUTOMOTIVE MATERIAL
READINESS COMMAND
SYSTEMS ENGINEERING DIVISION
ATTN DRSTA-GRA, MR. WALTER SLABIAK
WARREN, MI 48090

NAVAL ELECTRONIC SYSTEMS COMMAND
ATTN CODE ELEX 612, MR. CHET BRIER
ATTN CODE PME 124-31, MR. ALVIN H. SOBEL
WASHINGTON, DC 20360

NAVAL MATERIAL COMMAND
HEADQUARTERS NAVMAT (MAT-072)
ATTN MR. GLENN R. SPALDING
WASHINGTON, DC 20360

NAVAL OCEAN SYSTEMS CENTER
ATTN CODE 6343, MR. LEOPOLD J. JOHNSON
ATTN CODE 6343, DR. STANISLAW S. SZPAK
ATTN CODE 712, MR. JOSEPH F. MCCARTNEY
271 CATALINA BOULEVARD
SAN DIEGO, CA 92152

PROGRAM MANAGER, NLABS
POLLUTION ABATEMENT PROGRAM
ATTN MR. LEO A. SPANO
NATICK, MA 01760

NASA HEADQUARTERS
ATTN MR. JEROME P. MULLIN
ATTN DR. JUDITH H. AMBRUS
M.S. RTS-6
WASHINGTON, DC 20546

OFFICE OF NAVAL RESEARCH
ATTN CODE 472, DR. GEORGE A. NEECE, RM 624
ATTN CODE 472, DR. JERRY J. SMITH, RM 631
800 N. QUINCY ST
ARLINGTON, VA 22217

COMMANDER
DEPARTMENT OF THE NAVY
OFFICE OF NAVAL RESEARCH
ATTN CODE 429, LIBRARY
WASHINGTON, DC 20360

NAVAL SEA SYSTEMS COMMAND
ATTN CODE SEA 5433, MR. ALBERT HIMY
ATTN CODE PMS 395-A3, MR. RICHARD WALLACE
WASHINGTON, DC 20362

DAVID W. TAYLOR NAVAL SHIP R&D CENTER
ATTN CODE 2723, MR. JOSEPH A. WOERNER
ANNAPOLIS LABORATORY
ANNAPOPLIS, MD 21402

COMMANDER
DEPARTMENT OF THE NAVY
BUREAU OF NAVAL WEAPONS
ATTN MR. B. DRIMMER
WASHINGTON, DC 20360

COMMANDER
NAVAL WEAPONS CENTER
ATTN TECHNICAL LIBRARY
ATTN CODE 3852, DR. AARON FLETCHER
ATTN CODE 3275, MR. STEVEN E. AYLER
ATTN CODE 3626, MR. LOUIS L. D. PRACCHIA
CHINA LAKE, CA 93555

OFFICER IN CHARGE
NAVAL WEAPONS CENTER
ATTN DOCUMENTS LIBRARIAN,
DR. W. C. SPINDLER
CORONA LABORATORIES
CORONA, CA 91720

NAVAL WEAPONS SUPPORT CENTER
ELECTROCHEMICAL POWER SOURCES DIVISION
ATTN CODE 305, MR. MORRIS L. ROBERTSON
ATTN CODE 3053, MR. DONALD E. MAINS
CRANE, IN 47522

NAVAL SURFACE WEAPONS CENTER
WHITE OAK LABORATORY
ATTN CODE R-33, MR. DONALD L. WARBURTON
ATTN CODE R-33, DR. CARL E. MUELLER
ATTN CODE R-33, MS. CAROL FREEMAN
ATTN BEN LARRICK
ATTN S. [illegible]ALLECK
ATTN TECHNICAL LIBRARY
SILVER SPRING, MD 20910

AERO PROPULSION LABORATORY
AF WRIGHT AERONAUTICAL LABORATORIES
ATTN AFWAL/POO, MR. JAMES D. REAMS
ATTN AFWAL/POOC, DR. TOM MAHEFKEY
ATTN AFWAL/POOC, MR. DONALD P. MORTEL
ATTN AFWAL-POOC, MR. DON R. WARNOCK
ATTN AFWAL/POOC-1, MR. WAYNE S. BISHOP
ATTN AFWAL/XRPP, MR. ROBERT L. KERR
WRIGHT-PATTERSON AFB, OH 45433

AF CAMBRIDGE RESEARCH LABS
ATTN LQD, DR. RICHARD PAYNE
HANSCOM FIELD
BEDFORD, MA 01730

HEADQUARTERS AFSC/DLFP
ATTN MR. RICHARD E. SMITH
ANDREWS AFB, DC 20334

HQ, USAF/SAMI
WASHINGTON, DC 20330

ROME AIR DEVELOPMENT CENTER
ATTN RBES, MR. FRANK J. MOLLURA
GRIFFISS AFB, NY 13441

AF OFFICE OF SCIENTIFIC RESEARCH
AFOSC/NC, BLDG 410
ATTN DR. DENTON W. ELLIOT
BOLLING AFB
WASHINGTON, DC 20332

NATIONAL AERONAUTICS & SPACE
ADMINISTRATION
ATTN CODE RNW, MR. ERNST M. COHN
600 INDEPENDENCE AVE, SW
WASHINGTON, DC 20546

NASA GODDARD SPACE FLIGHT CENTER
SPACE POWER APPLICATIONS BRANCH
ATTN CODE 711, MR. LUTHER W. SLIFER, JR.
ATTN CODE 711.2, MR. GERALD HALPERT
GREENBELT, MD 20771

NASA JET PROPULSION LABORATORY
ATTN DR. ROBERT B. SOMOANO, BLDG 99
ATTN MR. IRVING STEIN, M.S. 198-220
4800 OAK GROVE DRIVE
PASADENA, CA 91109

NASA JOHNSON SC
ATTN CODE EP-5, MR. HOYT MCBRYAR
HOUSTON, TX 77058

NASA LEWIS RESEARCH CENTER
ATTN DR. MARGARET A. REID
(VICE CHAIRMAN)
M.S. 309-1
ATTN LIBRARY
21000 BROOKPARK RD
CLEVELAND, OH 44135

HQS, US MARINE CORPS
ATTN CODE LMA-4, MR. RICHARD E. ODERWALD
WASHINGTON, DC 20380

THE AEROSPACE CORP
ATTN MR. MARTIN J. MILDEN
PO BOX 92957
LOS ANGELES, CA 90009

BATTELLE MEMORIAL INSTITUTE
ATTN MR. BILL SPALSBURY
505 KING AVE
COLUMBUS, OH 43201

CATALYST RESEARCH CORP
ATTN V. KLASONS
1421 CLARKVIEW RD
BALTIMORE, MD 21209

EAGLE-PICHER INDUSTRIES
ATTN R. COTTINGHAM
PO BOX 47
"C" & PORTER STREETS
JOPLIN, MO 64801

ENGINEERING SOCIETIES LIBRARY
ATTN ACQUISITIONS DEPARTMENT
345 EAST 47TH STREET
NEW YORK, NY 10017

GENERAL ELECTRIC COMPANY
NEUTRON DEVICES DEPARTMENT
PO BOX 11508
ATTN R. SCWARC & R. WALTON
ST. PETERSBURGH, FL 33733

GLOBE UNION, INC.
PO BOX 591
ATTN MR. JOHN THOMAS
MILWAUKEE, WI 53201

MR. GEORGE J. METHLIE
2705 N. JEFFERSON ST
ARLINGTON, VA 22207

SAFT-AMERICA INC
ADVANCED BATTERY SYSTEMS DIVISION
ATTN KHUSHROW PRESS
200 WRIGHT AVE
COCKEYSVILLE, MD 21030

SANDIA NATIONAL LABORATORY
KIRTLAND AIR FORCE BASE, EAST
PO BOX 5800
ATTN A. BALDWIN
ALBUQUERQUE, NM 87185

UNION CARBIDE CORPORATION
CONSUMER PRODUCTS DIVISION
PO BOX 432
ATTN MR. L. ANZIVINO
BENNINGTON, VT 05201

THE UNIVERSITY OF WISCONSIN-
MILWAUKEE
ATTN PROF. C. D. HUBER
DEPARTMENT OF CHEMISTRY
MILWAUKEE, WI 53201

PENNSYLVANIA STATE UNIVERSITY
DEPARTMENT OF MATERIAL SCIENCE
COLLEGE OF EARTH & MINERAL SCIENCES
ATTN PROF. L. G. AUSTIN
UNIVERSITY PARK, PA 16802

US ARMY LABORATORY COMMAND
ATTN COMMANDER, AMSLC-CG
ATTN TECHNICAL DIRECTOR, AMSLC-TD
ATTN PUBLIC AFFAIRS OFFICE, AMSLC-PA

INSTALLATION SUPPORT ACTIVITY
ATTN DIRECTOR, SLCIS-D
ATTN RECORD COPY, SLCIS-IM-TS
ATTN LIBRARY, SLCIS-IM-TL (2 COPIES)
ATTN LIBRARY, SLCIS-IM-TL (WOODBRIDGE)
ATTN TECHNICAL REPORTS BRANCH, SLCIS-IM-TR
ATTN LEGAL OFFICE, SLCIS-CC

HARRY DIAMOND LABORATORIES
ATTN D/DIVISION DIRECTORS
ATTN DIRECTOR, SLCHD-RT
ATTN CHIEF, SLCHD-DE-F
ATTN CHIEF, SLCHD-DE-FM
ATTN CHIEF, SLCHD-DE-FT
ATTN CHIEF, SLCHD-DE-OE
ATTN CHIEF, SLCHD-DE-OM
ATTN CHIEF, SLCHD-DE-OP
ATTN CHIEF, SLCHD-DE-OS
ATTN CHIEF, SLCHD-DE-OW
ATTN MOORE, R., EL-PO-SP
ATTN SCHEINER, B., SLCHD-DE-OS
ATTN WYCKOFF, R. L., SLCHD-IT-EA
ATTN MCCARL, W. S., SLCHD-IT-EB
ATTN TOKARCIK, J. W., SLCHD-IT-EC
ATTN WEBSTER, W. H., JR., SLCHD-IT-EC
ATTN KITCHMAN, L. A., SLCHD-IT-EC
ATTN KUPER, W., SLCHD-DE-OP
ATTN NELSON, J. T., SLCHD-DE-OP
ATTN POESE, B., SLCHD-DE-OP
ATTN TEMPLEMAN, M., SLCHD-DE-OP
ATTN GOODMAN, R., SLCHD-DE-OS
ATTN DAVID, J. M., SLCHD-DE-OW
ATTN MILLER, J. W., SLCHD-DE-OW
ATTN LANHAM. C., SLCHD-TT
ATTN KRIEGER F., SLCHD-DE-OP (20 COPIES)

DTIC

FILMED

4-86

END